

UNIVERSITY ULM

MASTER THESIS

---

# Optical Properties of Colour Centres in Nanodiamonds

---

*Author:*  
Ou Wang

*Supervisor:*  
Prof. Fedor Jelezko  
Prof. Ute Kaiser

*A thesis submitted in partial fulfillment of the requirements  
for the degree of Master of Science*

*in the*

Institute of Quantum Optics  
Department of Science

October 11, 2016



## Declaration of Authorship

I, Ou Wang, declare that this thesis titled, "Optical Properties of Colour Centres in Nanodiamonds" and the work presented in it are my own. I confirm that:

- This work was done wholly or mainly while in candidature for a research degree at this University.
- Where any part of this thesis has previously been submitted for a degree or any other qualification at this University or any other institution, this has been clearly stated.
- Where I have consulted the published work of others, this is always clearly attributed.
- Where I have quoted from the work of others, the source is always given. With the exception of such quotations, this thesis is entirely my own work.
- I have acknowledged all main sources of help.
- Where the thesis is based on work done by myself jointly with others, I have made clear exactly what was done by others and what I have contributed myself.

Signed:

---

Date:

---



UNIVERSITY ULM

*Abstract*

Quantum Optics  
Department of Science

Master of Science

**Optical Properties of Colour Centres in Nanodiamonds**

by Ou WANG



# Contents

<b>Declaration of Authorship</b>	<b>iii</b>
<b>1 Motivation and Background</b>	<b>1</b>
1.1 Quantum information processing and Qubit candidates . . . . .	1
1.2 Silicon vacancy as a Qubit candidate . . . . .	2
1.3 Silicon vacancies in nanodiamonds . . . . .	3
1.4 Motivation of the thesis . . . . .	4
<b>2 Sample preparation and Experiment Apparatus</b>	<b>7</b>
2.1 Sample information . . . . .	7
2.2 Sample preparation . . . . .	7
2.2.1 preparation of the substrate . . . . .	7
IIa diamond as substrate . . . . .	7
Focused Ion Beam milling . . . . .	8
Acid cleaning . . . . .	9
2.2.2 Spin-coating of the sample . . . . .	10
Spin-coating theory . . . . .	10
spin-coating practice . . . . .	11
2.3 experiment apparatus . . . . .	11
The initial Setup . . . . .	11
Methods for characterisation . . . . .	12
<b>3 Surface treatments</b>	<b>15</b>
3.1 Oxidation . . . . .	15
3.1.1 first Oxidation . . . . .	15
3.1.2 Second Oxidation . . . . .	18
3.2 H termination . . . . .	19
<b>4 Result and Discussion</b>	<b>23</b>
4.1 Compilation of data . . . . .	23
4.2 Nanodiamond size and spectral stability . . . . .	23
4.3 Excitation power and spectral stability . . . . .	24
4.4 Temperature and spectral stability . . . . .	25
4.5 Excitation polarisation and spectral stability . . . . .	25
4.6 Aerobic Oxidation and Spectral stability . . . . .	26
4.7 Hydrogen termination and Spectral stability . . . . .	26
4.8 Discussion . . . . .	27
<b>5 Conclusion and outlook</b>	<b>41</b>
5.1 Conclusion . . . . .	41
5.2 Outlook . . . . .	41
<b>A Appendix Title Here</b>	<b>43</b>

<b>Bibliography</b>	<b>45</b>
---------------------	-----------

# Chapter 1

## Motivation and Background

### 1.1 Quantum information processing and Qubit candidates

The bit is the basic unit of information in computing and digital communications. A bit can have one value, which can be 1 or 0, that represents the logical states in a 2-level logic system. In modern digital computers, these two states exists as low and high voltages in highly integrated circuits. Just like a bit for classical computing, a qubit is the basic unit of information in Quantum Information Processing (QIP), which encodes 1 and 0 into 2 distinguishable quantum states. As the qubits behave in the manner of quantum mechanism, it gives rise to the phenomena of superposition and entanglement, the computing power increases exponentially while more qubits adding up together. Previous difficult tasks in classical computing such as simulation of quantum systems or factoring of numbers would be finished quickly and efficiently by quantum computers.

For the realisation of a quantum computer, the first priority is to find a suitable candidate as qubit. Five principles have been brought up for the candidates choosing by (DiVincenzo and IBM, 2000):

1. A scalable physical system with well characterized qubits
2. The ability to initialize the state of qubits to a simple fiducial state
3. Long relevant decoherence times, much longer than gate operation time
4. A "universal" set of quantum gates
5. A qubit-specific measurement capability

Color centres are optically active impurities that are responsible for the colors in crystals that are transparent due to large band gap. They are atom-like solid systems that, with appropriate electronic structure and symmetry in crystal, can be the candidates for qubits. Additionally, it is practical to require a long enough coherent time for information storage, thus quantum information processing can happen.

Lots of research has been done with the negative charged nitrogen vacancy ( $\text{NV}^-$ ), which has excellent spin properties at ambient condition (Childress, Walsworth, and Lukin, 2014), it has also been proved that it is possible to execute an all optical access to its spin. (Bassett et al., 2014; Buckley et al., 2010; Santori et al., 2006). Yet due to the transform of symmetry during the excitation process,  $\text{NV}^-$  has a big phonon side band following the zero-phonon line (ZPL). Moreover, the  $C_{3v}$  symmetry leaves the color centre vulnerable towards the environment electric field, resulting in spectral diffusion, which is caused by the flipping of charging state. These disadvantages has reduced the generation rate of coherent photon generation

rates and limit the development of NV-quantum networks (Rogers et al., 2014a).

## 1.2 Silicon vacancy as a Qubit candidate

Negative charged Silicon vacancy centres ( $\text{SiV}^-$ ) are considered as the next promising qubit candidate after  $\text{NV}^-$ . It has irresistibly excellent optical properties, and is also possible to achieve an all optical intiallizaiton, read out and coherent preparation.

$\text{SiV}^-$  has a  $D_{3d}$  symmetry with the symmetry axis along the  $\langle 111 \rangle$  crystal direction. The color center consists of a substital Silicon atom and a carbon vacancy. Due to the size difference between Silicon atoms and carbon atoms, it is expected that the Silicon atom will sit between 2 lattice site instead of on a lattice site(Goss et al., 1996; Gali and Maze, 2013). The inversion symmetry offers  $\text{SiV}^-$  extra shielding from the small electric field fluctuation.

Experimentally it is observed that the  $\text{SiV}^-$  has outstanding optical properties, 70% of its fluorescence coupled into a sharp ZPL at 1.68eV Wang et al., 2006. At cryogenic temperature this ZPL can be resolved with a fine structure of 4 lines. These four lines correspond to the electronic transitions between the ground state and the first excited state of  $\text{SiV}^-$ . Theoretical calculation based on group theory and ab initio methods offer us a model of the  $\text{SiV}^-$  electronic structure with a ground state of 2-fold degeneracy and even parity, a first excited state of 2-fold degeneracy of uneven parity and a second excited state of no degeneracy with even parity. (Goss et al., 1996) This calculation fits the observation as only the electronic transition between levels of different parity is allowed, due to the -1 parity of photons, thus only the 4 transitions between the first excited state and the ground state would be allowed, corresponding to the 4 line structure of ZPL. Since this is a E to E transition, no dramatic symmetry change has been involved, less phonon would be involved in the relaxation, which fits the observation of the sharp ZPL with small phonon side band.

Rogers et al. showed the probility to read out and coherently prepare electronic spin in individual  $\text{SiV}^-$  centers via resonance excitation. As shown in the 1.2 The  $\text{SiV}^-$  was first initialized by resonantly pumping the spin-flipping transition D1 that is weakly allowed due to the off axis residue of the magnetic field, this is done with applying a laser pulse that resonant to transition D1. After a dark interval the spin state was read out using a laser pulse on the cycling transition D2. The leading edge peak from D2 pulse will decrease with the increase of dark interval approaching an minimum. From this the spin relaxation time T1 has be calculated as  $2.4 \pm 0.2\text{ms}$ . With the similar pulse measurement, the orbital T1 has been measured as  $38 \pm 1\text{ns}$ . The fact that the orbital T1 is much shorter than spin T1 indicates that the orbital relaxation is highly spin conserving, indicates that this is a phonon transition. The temperature dependency measurement reveals that the orbital rate increase linear with the temperature until 22K, which indicates a single-phonon mechanism of orbital relaxation.(Rogers et al., 2014a; Orbach, 1961; Rogers et al., 2014b; Scott, 1962)

Further coherent population trapping (CPT) was carried out by tuning the pump laser to transition D2 while scanning across the transition D1

using the probe laser. The spin coherence time was then measured to be  $35 \pm 3$  ns. This short coherence time is connected to the dephasing caused by the rapid orbital relaxation.(Rogers et al., 2014a)

Practically, as mentioned before, a qubit candidate ideally needs to have long enough coherent time for the implementation of operation and read out, in this sense, the short coherent time of  $\text{SiV}^-$  drew it back from being an competitive qubit candidate.

Several ideas of acquiring longer coherence time has been taken into consideration. While most of them can be classified into two main approaches: avoid orbital relaxation caused electron spin dephasing by accessing the nuclear spin in  $\text{Si}^{29}$  (Dietrich et al., 2014) or eliminate the single phonon that has been involved in the orbital relaxation.

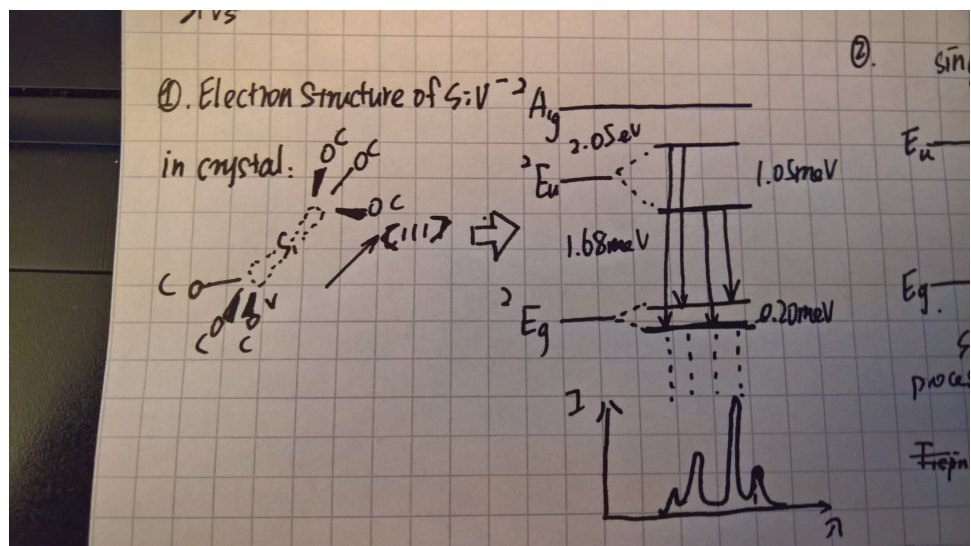


FIGURE 1.1

### 1.3 Silicon vacancies in nanodiamonds

As mentioned, one vital problem to solve if we want to use  $\text{SiV}^-$  as a qubit is that, the coherent time has been limited by the rapid orbital relaxation. This is caused by the transition between the degeneracies of ground state which was driven by a single phonon. The elimination of such phonon is an direct approach towards the solution.

The inhibit of orbital relaxation rate can be achieved by the shrinkage of nanodiamond size. Considering the nanodiamond in vacuum as a 3D phonon cavity, a discrete phonon spectrum would be generated. (Albrecht et al., 2013) A particle size smaller than half of the transition phonon length would inhibit the orbital relaxation time. (Kleppner, 1981)

Currently 3 major techniques are employed in the field of nanodiamond fabrication: denotation, chemical vapor deposition (CVD), and high pressure high temperature method (HPHT), while the impurity atoms can be mixed in the beginning or implanted via ion implantation. Since the denotation method produced highly defective diamonds and ion implantation introduces inner strain, for the  $\text{SiV}$  containing nanodiamonds, HPHT method and CVD method are the top choices.

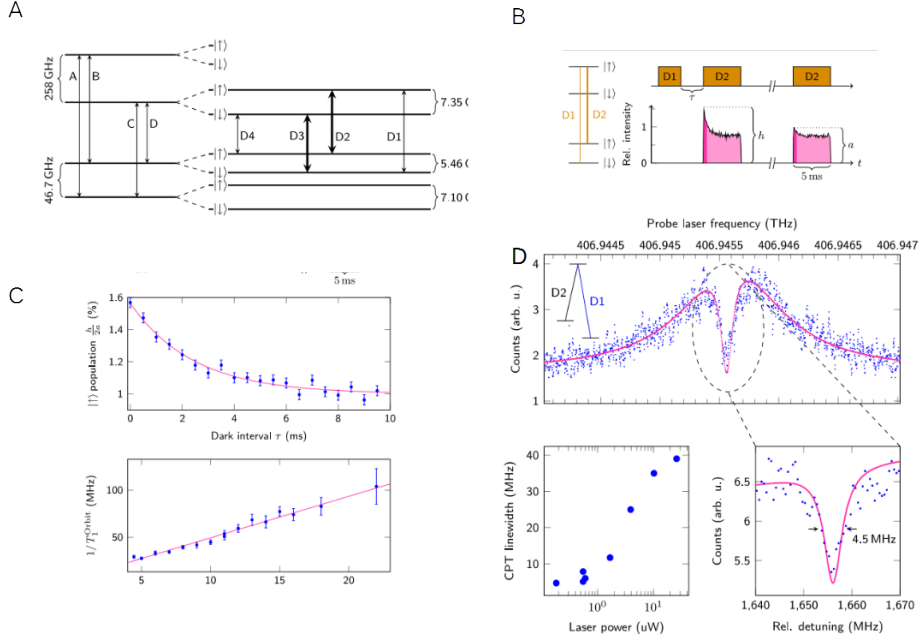


FIGURE 1.2: A: Zeeman splitting of the spin=− $\frac{1}{2}$  electronic states. B: A laser pulse resonant to transition D1 flips the spin without producing measurable fluorescence. The initialized spin state can be read out using a laser pulse on the cycling transition D2. C: (Upper) The reduction of  $h$  with increasing  $\tau$  gives the spin relaxation time at spin  $T_1 = 2.4 \pm 0.2\text{ms}$ . Interpreting the asymptotic limit  $a$  to correspond to thermal spin population suggests a spin initialization fidelity of  $h_{\tau=0}/2a = 78\%$ . (Lower) Similar pulsed measurements give the orbital relaxation time at 4.5K as orbital  $T_1 = 38 \pm 1\text{ns}$ . The orbital relaxation rate  $1/T_1$  increased linearly with temperature.

The principle of the CVD method is to disintegrate the CVD fabricated diamond film, while the HPHT method initializes an phase transition of carbon at high temperature and high pressure. Previously, comparison between the PL spectra of silicon doped polycrystalline diamond films obtained by the CVD method and diamond single crystals grown at a pressure of 6 GPa from a nickel melt at 1500°C has been carried out, and it was demonstrated that the HPHT diamonds exhibit narrower SiV<sup>−</sup> ZPL lines than CVD fabricated ones (Clark et al., 1995). HPHT nanodiamonds carrying SiV<sup>−</sup> with almost lifetime-limited line widths has been reported by Uwe Jantzen. (Jantzen et al., 2016)

## 1.4 Motivation of the thesis

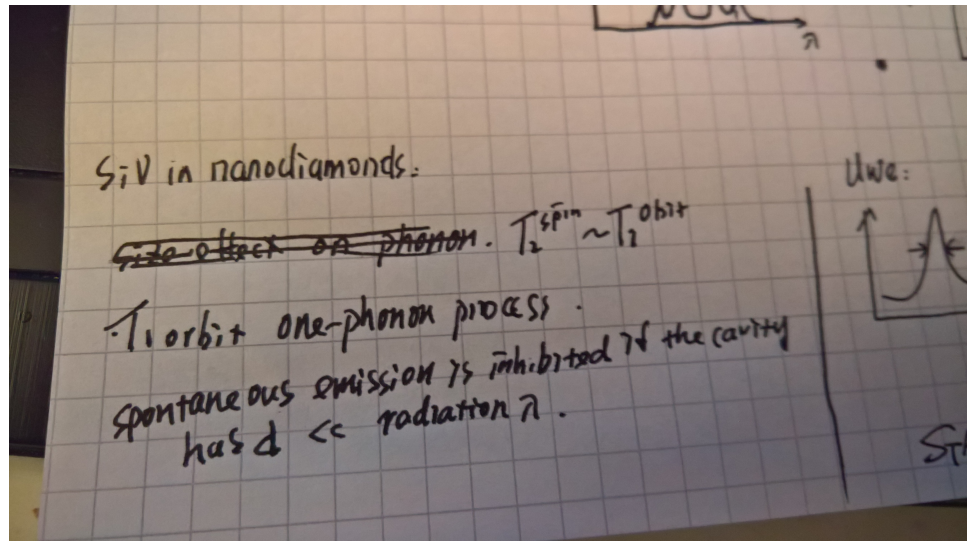


FIGURE 1.3

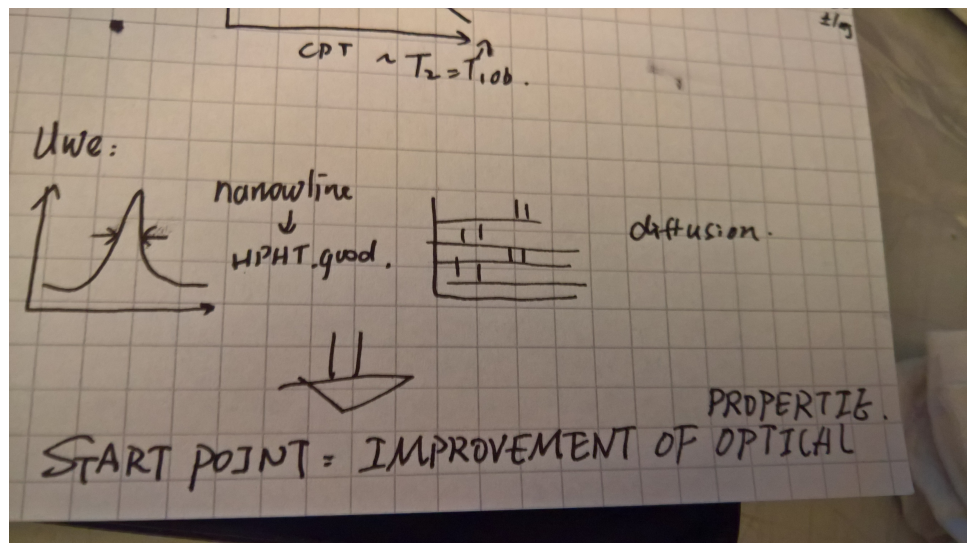


FIGURE 1.4

The idea of generating longer coherent time via phonon inhibition in nanodiamonds has been put forward, yet not experimentally proved. (Jantzen et al., 2016) has reported the narrowest ZPL in nanodiamonds, but the spectral shift/diffusion is a great obstacle preventing people from measuring the orbital relaxation time.

The mechanism behind the spectral diffusion is yet not clear, but due to the high surface to volume ratio of nanodiamonds, it is highly possible that this phenomenon is connected with the surface conditions. (Jantzen et al., 2016)

To step further in the research direction of SiV<sup>-</sup> in nanodiamonds. The current goal is to suppress the spectral diffusion, enabling following measurements (Orbital T1, Spin T1, CPT, etc.) to prove the possibility of acquiring longer coherent time.



## Chapter 2

# Sample preparation and Experiment Apparatus

### 2.1 Sample information

The nanodiamonds that are used as sample in this project was synthesised from a trinary mixture of naphthalene ( $C_{10}H_8$ ), highly fluorinated graphite ( $CF_{1.1}$ ) and Tetrakis(trimethylsilyl)silane( $C_{12}H_{36}Si_5$ ) at a pressure of 8 GPa and a temperature of 1100°C. These nanodiamonds carry optically active SiV and NV. The presence of NV is the result of spontaneous doping from the synthesis procedure, more specific, is due to atmospheric nitrogen adsorbed on the surface of naphthalene powder.(Davydov et al., 2014)

To obtain cleaner and more size-refined nanodiamond, the sample was then centrifuged and divided into four batches following the condition in table 2.1. in between each step, the residue was re-dispersed in 1ml of microwater. The average size of the nanodiamonds in batch 1 is expected to be the smallest, and the ones in the 4th batch are expected to have the largest size.

### 2.2 Sample preparation

#### 2.2.1 preparation of the substrate

##### I<sub>IIa</sub> diamond as substrate

To choose a proper substrate for the nanodiamond sample, a few principles need to be considered.

TABLE 2.1: Centrifuging conditions for nanodiamond size selection

Batch Number	Centrifuging Condition
1	2000rpm 1min
2	1000rpm 1min
3	500rpm 1min
4	300rpm 1min

1. Low background fluorescence. It is always vital to obtain a decent signal to noise ratio in any kind of measurements. As for our case, the emission(fluorescence) from silicon centers are the target, thus it is desired to lower the background fluorescence as much as possible.
2. Good heat conductivity at low temperature. From previous calculation done by Uwe Jantzen (Jantzen, 2015), we know that the temperature difference  $\Delta T$  between the bottom of the substrate and nanodiamonds(which are spin coated on the surface of the substrate) can be estimate as  $\Delta T = \frac{\sigma \cdot d \cdot T^4}{k}$ , where  $\sigma$  is the Stefan–Boltzmann constant,  $d$  is the thickness of the substrate and  $k$  is the thermal conductivity. To resolve the fine feature of silicon vacancy ZPL, we want to characterise the nanodiamond sample at a temperature that is lower than 30K for spectrometer and 10K for PLE.
3. No distracting spectral features. Misleading peaks from fluorescence of the substrate would be the least wanted when we want to character a sample spectrally. In many cases, this is related to the raman-scattering of the photons, which highly depends on the crystal structure of the substrate.
4. Refractive index. Inam et al calculated the relative emission rate for radiating dipoles near an interface between two dielectrics with Finite-difference time-domain method. (Inam et al., 2011) The result demonstrates that, when the dipole lies perpendicular or parallel to the substrate, the emission rate from a interface with lower relative refractive index is always higher than that from a interface with higher relative refractive index. To increase the emission rate, a substrate with lower refractive index would be preferred.

Taking these principles into consideration, Many typical materials has been excluded such as glass/quartz (distracting raman shift lines) and Sapphire (also a distracting raman shift line, and impurity induced emission that calls for extra attention when picking the optical filters). Here we use IIa diamond, which has a low impurity density(resulting in low background fluorescence intensity), relatively low refractive index (2.4 to 2.7), good thermal conductivity ( $\Delta T = 4.17 \cdot 10^{-2} K$ ) and a raman shift at  $1332 cm^{-1}$  that causes no distraction on our observation.

### Focused Ion Beam milling

In order to make it more convenient to trace the nanodiamonds, markers were hab previously been cut onto the surface of the IIa type diamond substrate.Jantzen, 2015 As is shown in the 2.1, the focued ion beam bombards the surface of diamond away and leaves behind markers that are visible in optical microscopy images and SEM images, as well as confocal microscopy images. The impact of ion may also introduce new defect into the substrate, which will be discussed later.

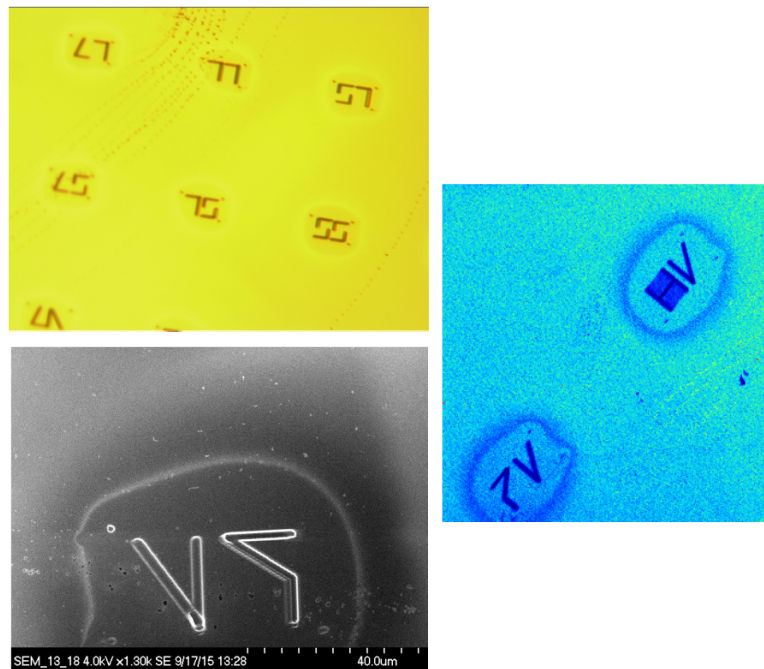


FIGURE 2.1: Pictures of markers obtained from FIB, which are placed following the order of numbers. They are visible in optical microscopes, confocal microscopes as well as SEM

### Acid cleaning

To make sure that the NDs dispersion can evenly spread and eventually settled on the substrate, a smooth, clean and hydrophilic surface is important.

Acid boiling is a very practical way of diamond substrate cleaning and involves boiling the diamond in a mixture of three strong mineral acids: sulfuric acid, nitric acid and perchloric acid. This mixture has very strong ability of oxidizing.

After assembling the setup, we initialize the reaction by heating the mixture to a temperature where it is mildly bubbling. The substrate would be stay inside the boiling tri-acid mix for 4h. After the acid boiling, the sample should be removed from the flask and rinsed with pure water, after which a rapid blow dry with clean air is compulsory. The mixture of strong mineral oxidizing acids can remove most of the adhesions on the surface of diamond substrate, leaving a clean hydrophilic surface. This oxidizing procedure will lead to the formation of carbonyl and carboxyl groups. Although via acid boiling, most of the attachments on the surface can be removed, there is still very high chance to introduce other contaminations from the water and the air while the sample is still wet. Thus it is highly recommended to dry the sample rapidly after the cleaning procedure with clean pressed air. A acetone boiling session before spin-coating in the clean room is also important.

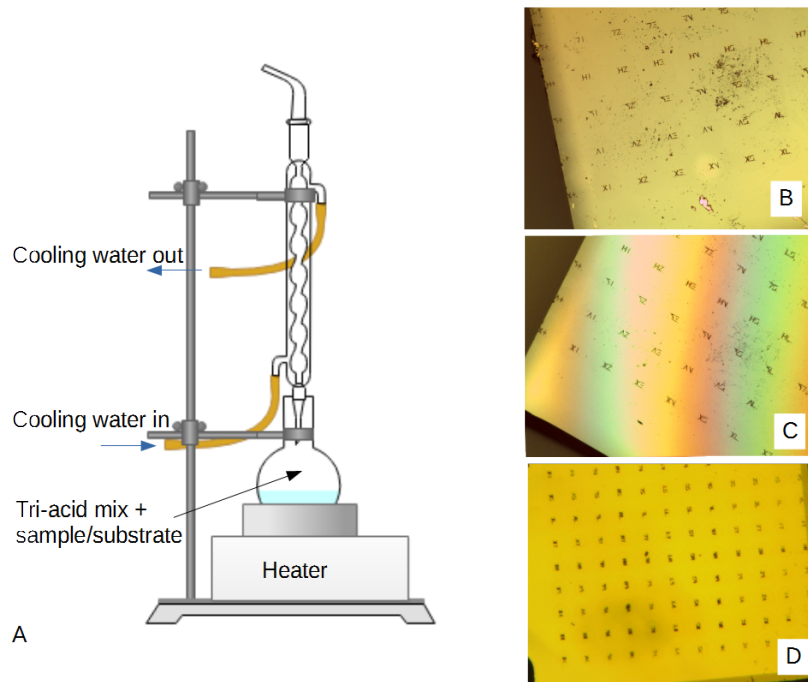


FIGURE 2.2: a) setup up of acid cleaning. b)substrate 207 before cleaning. c) substrate 207 after acid boiling. d) acid cleaned substrate 207 after acetone boiling in the clean room.

## 2.2.2 Spin-coating of the sample

### Spin-coating theory

Spin coating is the method of sample preparing that mainly contains 2 steps. The first involves spreading. In this step, a volume of liquid containing the particle that we want to coat with is dropped on the surface of the substrate, driven by the centrifugal force from the rotational movement of the substrate, the liquid would be spread evenly on the surface. The second step is the evaporation of the 'solvent'. While the sample stage rotates, the 'solvent'(In our case is not a real solvent, since nanodiamonds never really desolve.) would evaporate, leaving the particle/molecules that are wanted to be coated on the substrate.

In the spin coating session, the following factors were found to be important.

1. spin speed: generally the thickness of the liquid layer  $t$  is proportional to the inverse of the angular velocity  $\omega$  squared  $t \sim \frac{1}{\sqrt{\omega}}$ , higher speed would help with forming a more uniform layer, yet this also means a smaller volume of solution, which would lead to lower density of nanodiamonds on the surface. On the other hand, with lower speed the probability of aggregation would increase, which is also what we want to prevent.

2. volume of the 'solution': larger volume means longer drying time, which would increase the probability of aggregation and losing nanodiamonds, while smaller volume leads towards lower density of nanodiamond and more difficulty when trying to drop it with a pipette.

3. type of solvent: The type of solvent, viscosity and boiling point are important for the dispersion of nanoparticles inside solution, the spreading

of the solution while spin coating and the rate of evaporation.

4. surface condition of the substrate. High contact angle is a obstacle towards the spreading of the solution, high roughness or inappropriate surface group of the substrate can result in poor wettability from the solution.

### **spin-coating practice**

Throughout the project, with the help of Andrea Kurz, several combination of these factors have been has been tried out on different samples.

1. 35ul Chloroform with 1ul of nanodiamond, take 2ul of this kind of mixture and drop it on the substrate in one time. The spin speed is 5000rpm and the duration is 40s. (Sample 1506, 1507)

2. 30ul Chloroform with 1ul of nanodiamond, 2ul of mixture, apply in one time, 5000rpm and 40s. (Sample 1508, 1509)

3. 30ul Choloroform and approximately 120ul of water with 1ul of nanodiamond, 2ul of mixture, apply in one time, 8000rpm and 40s. (Operated on substrate207 and found no SiV<sup>-</sup> signal later.)

4. 30ul Choloroform and approximately 120ul of water with 1ul of nanodiamond, 10ul of mixture, apply in 5 times, each time 2ul, after each application, spin with the speed of 5000rpm and duration of 40s. (sample 1510, 1512)

All the 3 methods other than method III produced samples with SiV<sup>-</sup> containing points of interest. But among them, the method IV offers the highest SiV<sup>-</sup> density.

## **2.3 Experiment Apparatus**

### **The initial Setup**

The setup can be coarsely separated into laser source, confocal microscope(with APD and spectrometer as detector), flow cryostat and vaccum pump, these four parts are all sketched in Fig. 2.4.

While the absorption spectrum shows the highest off resonance absorption around 530nm (Iakoubovskii and Adriaenssens, 2000; Albrecht et al., 2013; Rogers et al., 2014b), the ZPL of silicon vacancy lies around 737nm. We chose to use green laser of wavelength 532nm as the laser source for photoluminescence spectrum and Titan Sapphire laser with the ability of scanning around 737nm as the laser source of photoluminescence excitation. These two methods will be more detailed written about in the following paragraphs. The lasers are coupled into the same photonic crystal fibre, which guides the beam towards the optical table.

The second part is the confocal microscope, which is a very useful tool for imaging of samples that emits fluorescence, such as SiVs. Compared with fluorescence microscope, as sketched in Fig. 2.5, the confocal microscope uses a pair of convex lens and a pinhole that conjugates to the lens to achieve the increase of resolution and signal to noise ration. In the setup, there are two possibilities of signal detection, controlled by a flipping mirror, we can choose to count the photons with a pair of APD, or record the spectrum with a spectrometer. As the resolution of fine splitting of SiV ZPL needs to be measured in low temperature, the motorized sample stage is

placed in a flow cryostat, the objective lens is also inside the cryostat. As the name mentioned, the decrease of temperature in this cryostat is achieved by the flow of cold, boiling liquid Helium, a transfer line connects the Helium dewar and the inlet of the helium cooling circulation inside the cryostat. The sample sits right on the cold finger, with proper method of mounting and substrate, the temperature can be brought to as low as 3.5K(need to check).

To reach cryogenic temperature, it is vital to cut off the heat exchange between the sample and the world outside the cryostat, since air and stainless steel(the material of the cryostat wall) can both conduct heat, a UHV condition need to be met. In our setup, it is realized by the pumping system of a back pump and a turbo pump. The back pump pre-pumps the pressure until it meets the working condition for turbo pump.

### **Methods for characterisation**

With the mentioned setup, we are able to characterise the sample with following basic methods.

**Photoluminescence** Photoluminescence detects the emission after the absorption of photons. In our case, we use the 532nm laser to excite the sample, which would bring the SiV<sup>-</sup> to the second excited state, while the electronic transition between 2 energy levels of the same parity is not allowed, it is possible to conduct the transition between such kind of 2 energy level via the creation and annihilation of phonons, thus it will be the 4 transitions between the first excited state and the ground state that we are expect to record in the spectrum .

The resolving power of a grating in a spectrometer depends on the width of the grating, the centre length to be resolved and the geometry of the use condition. In our setup, a resolution of 16GHz can be achieved, which is capable of observing the 4 line structure in SiV<sup>-</sup> ZPL, but not enough to resolve a peak with the width of the lifetime limit.

**PLE** When PL excites the sample with a laser of single wavelength to obtain the information about multiple emissions, PLE, on the contrary, excites the sample with various wavelength and monitors the photon emission from the side band to characterise a single transition. The resolution of PLE depends on the resolution of laser, with the Matisse Titan-Sapphire laser(linewidth of 50kHz), it allows us to resolve single electronic transmission in SiV<sup>-</sup> with life time limited line width, as well as to obtain better signal to noise ratio.

**time resolved PL spectra** It is very inconvenient monitoring the spectral diffusion in the scale of nm with PLE. To help characterise the spectral diffusing behaviour of SiV<sup>-</sup>, we improvised the time-resolved PL spectra. By stacking the sequentially taken spectra in the order of time, we can visualize and estimate the spectral diffusion in a more coarse but convenient way.

Departing from the initial setup, a few alternations have been done during the project, which would be discussed in detail in the following up contents.

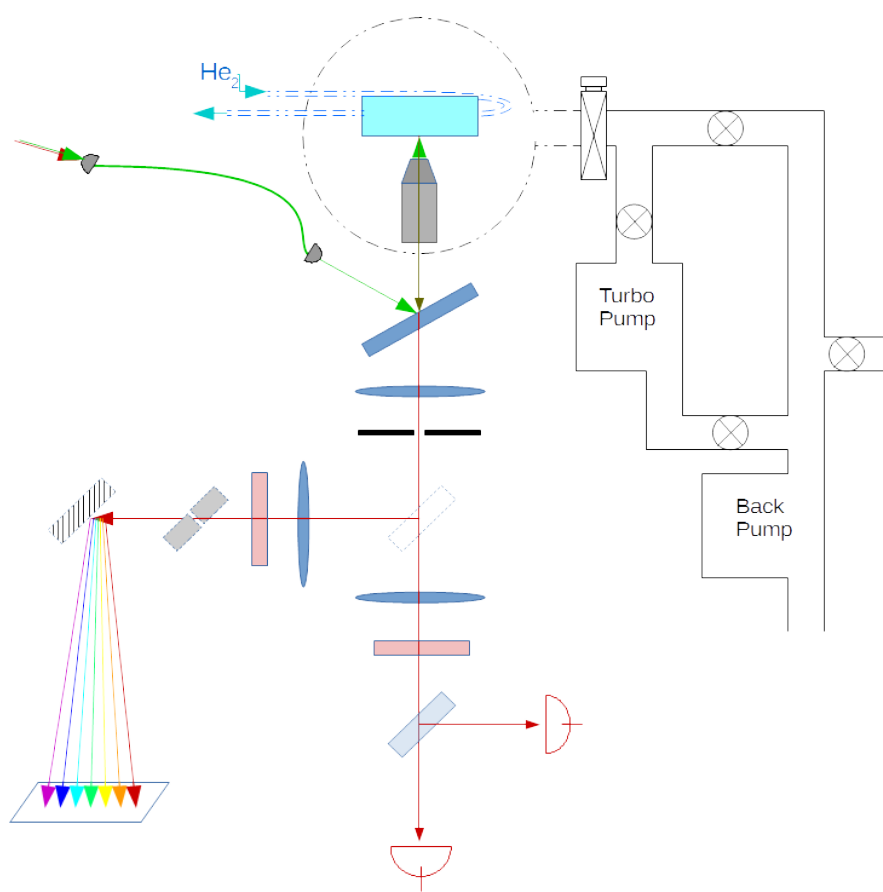


FIGURE 2.3: A sketch of the initial setup.

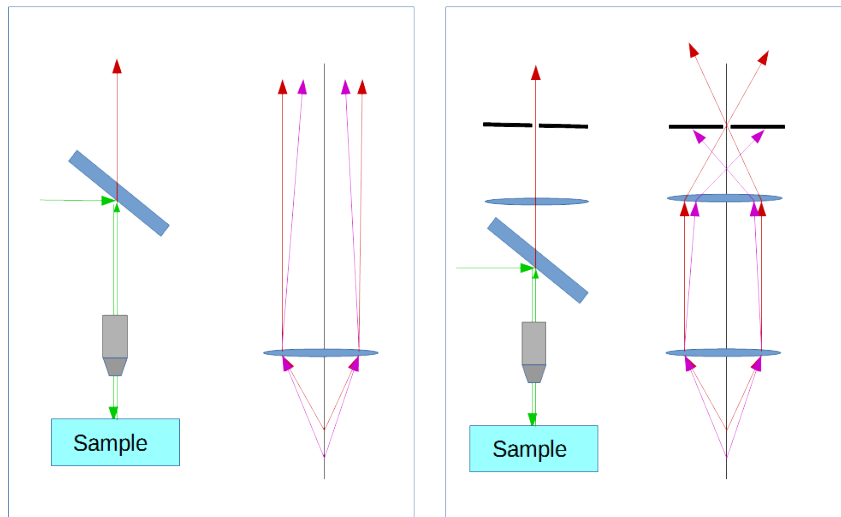


FIGURE 2.4: A)In a typical fluorescence microscope, the back ground fluorescence will also be collected. b)In the confocal microscope, with the help of a lens conjugating pin hole, a large fraction of the fluorescence from non-focus plane will not get through by the pinhole.

# Chapter 3

## Surface treatments

### 3.1 Oxidation

Room temperature oxidization is a common way of nanodiamond purification. With different oxidizing temperature, different types of impurities can be removed from the surface of the nanodiamond, ranging from water and physisorbed organic impurities, amorphous carbon, and graphitic shells and ultimate the  $sp^3$  phase of diamond (T. Gaebel, 2012). After the oxidation, carbonyl and carboxyl groups are formed on the surface (Wolcott et al., 2014). Several paper have mentioned temperature choices for oxidation aiming at impurity removal.(Osswald et al., 2006; Wolcott et al., 2014; T. Gaebel, 2012) During the master's thesis period, 2 different oxidation has been examined.

#### 3.1.1 first Oxidation

As reported, it is possible to achieve the removal of  $sp^2$  carbon without any oxidation on  $sp^3$  carbon via aerobic oxidation with temperature between  $375^\circ C$  and  $450^\circ C$ . Osswald et al., 2006 With temperature lower than  $500^\circ C$ , the size reducing rate of nanodiamond is lower than 1nm/h. (T. Gaebel, 2012) As our first treatment, we carried out a two step oxidation on sample 1508 and 1509, to achieve the complete removal of graphitic defect on the surface and light oxidation on the surface. Sample 1508 was spin coated with nanodiamond batch2, sample 1509 was spin coated with nanodiamond batch1.

The aerobic oxidation is carried out in a tube furnace and it is done with the help of Markus Mohr. The tube furnace consists of a glass tube connected to the room atmosphere and heating coils around the glass tube. The glass tube can be slide in or out of the heating coils. We put our sample inside a ceramic sample holder and put the holder into the glass tube carefully, after the temperature has been raised to  $460^\circ C$ , the glass tube was slide into the heating coils. The sample was oxidized at  $460^\circ C$  for 90min,then  $480^\circ C$  for 40min.(Neu et al., 2013) After the Oxidation, the glass tube was slide out and the sample stayed inside the tube until it reached room temperature.

Before the oxidation, the samples was first mapped with a room temperature setup that resembles fig. 2.4, but without vaccum pump and cryostat. To make a map of  $SiV^-$  containing points of interest, it was first taken, a scan with green laser while the fluorescence was recorded by APD, which offers us a confocal microscopy image of the sample, then the photoluminescence spectra of the bright spots were taken, coordinates of those ones

with a sharp peak at 737nm saved as points of interests for the reference of further examine.

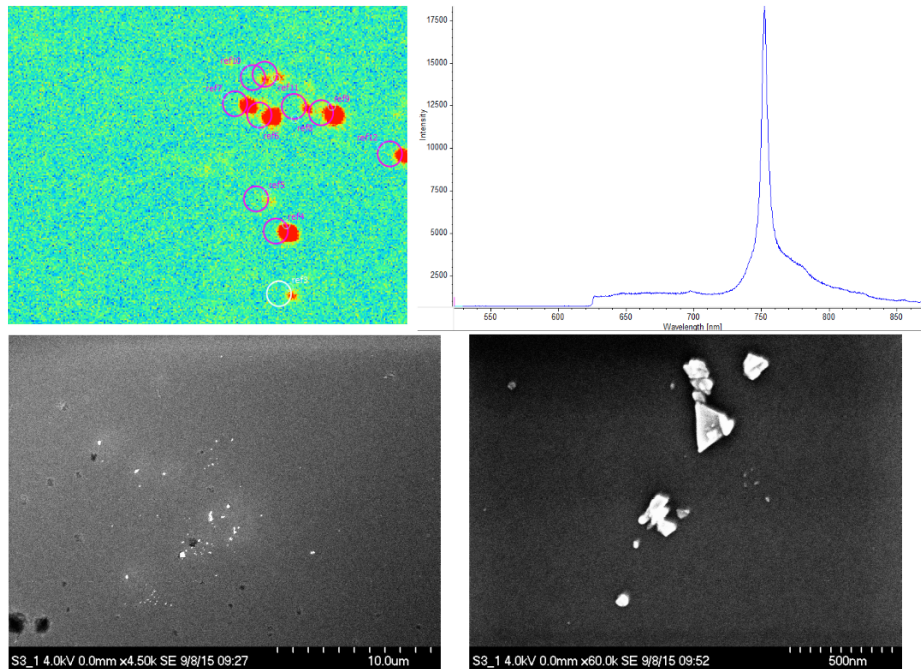


FIGURE 3.1: A)confocal image of a region of interest. The bright spots with circle markers are points of interest. B)Room temperature spectrum of a poi recorded by spectrometer. C)the roi in SEM. D)ref10 and 11 in SEM.

Once the map was acquired, we bring the samples to the electron microscope center and observed the regions of interest with SEM. SEM showed that, sample1508 contains more big single crystals that are larger than 300nm and clusters, while sample 1509 contains more single crystal with under 200nm sizes. This proved that the size selection via centrifuging has worked.

The samples was then attached to an cold finger and the placed inside the cryostat, after UHV condition has been achieved, the helium transfer was started, which would brought the temperature of the sample down to 4.8K. Most of the mapped pois are refound. Excitation with 532nm green laser double checked the existence of SiV. After the confirmation, it has been tried to carry out a resonance excitation with Titan Sapphire laser, when observing a few points of interest next to marker 5A in sample1509, it was noticed that while scanning the red laser across the line with the help of very low amount of 532nm for repopulation, a spectral diffusion of 6GHz in 15Min has been observed. To exclude the possibility of instrumental error, PLE has been operated on the bulk diamond sample with also SiV inside, where no spectral diffusio has been observed 3.2. It has also been noticed that the increase of green laser power can cause more severe spectral drift/jump. In a case when the power green laser is brought up for a better refocus, the line has shifted totally out of the range of the spectra scan, and didn't recover in 10min. This observation brought difficulty in the measurement of orbital T1, since we always need to initialize the obital states with green laser, and this spectral diffusion that is related to the application of green laser can result in the fail of hitting the resonant wavelength, since

it is technically difficult to refind the line and adjust the wavelength of the resonance laser coordinately.

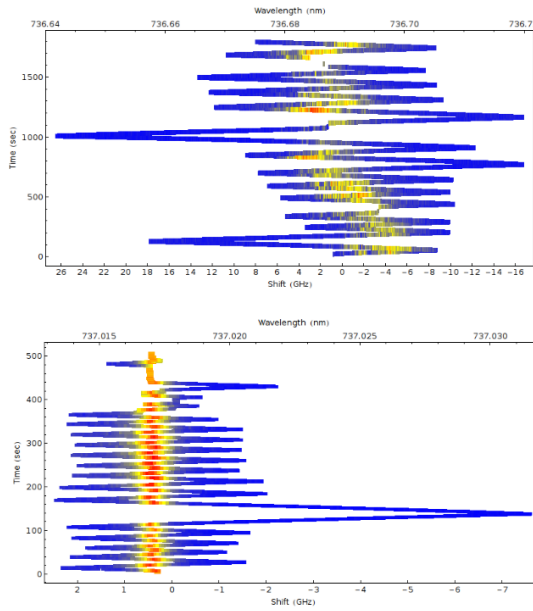


FIGURE 3.2: PLE scan over time on A) ref5A\_014 from sample1509 and B) a SiV<sup>-</sup> site from bulk diamond sample 33b. No significant spectral diffusion been found in bulk diamond sample, which exclude the possibility of instrumental error.

After the obeservation above, we want to study more about this spectral diffusion behaviour that is associated with the green laser. We noticed that the sudden jump/diffusion when more green power is applied can be larger than 20GHz, maybe it is easier to track the movement of the lines with the high resolution grating of spectrometer than with PLE.

To observe the diffusion with a spectrometer, we introduced time-resolved photoluminescen spectrum, which has been described in last chapter. Due to the technical problem, our motorized sample stage can not move ideally in the vertical direction anymore, which has limited our region of observation. This time we refound the ROI around the marker 4C. And recorded the time-resolved spectrum. A session is set to be 60 spectra taken consecutively. At first, to feel the long term diffusing better, 3 sessions, with a refocus after each, are undergone for each points of interests. Since line diffusion in PLE gets wider when raising the green laser power, we excite the sample with 500uW power in front of the objective lens to obtain more diffusion. As a result, line diffusion up to 1nm has been observed. Sequentially

we decrease the input power to examine the power dependency of spectral

Taking the samples out of the furnace, we noticed that the surfaces of the samples turned very dirty. It is yet not clear, what the contaminations are, are they intrinsic or are they extrinsic. A possible explanation is that, the contamination comes from the glass tube of tube furnace, that the residues of previous treatments has attached to the inner surface of the tube and evaporized again, depositing on the surface of our sample. Further improvement of oxidation operation has been done in our second oxidation test, and will be mentioned in the next part of the thesis.

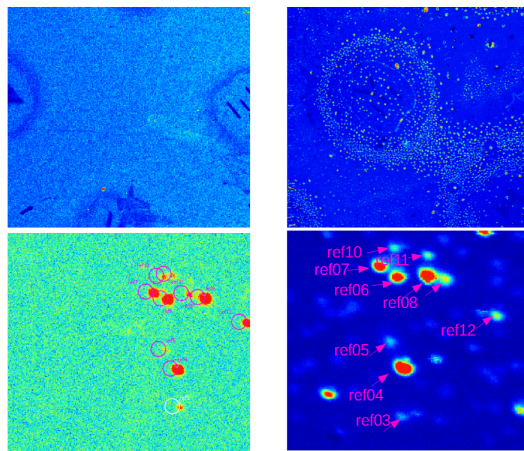


FIGURE 3.3: A) region of interest next to marker 3C of sample 1508 before oxidation B)the same region of interest after oxidation C) Points of interest from the ROI before oxidation D)points of interest after oxidation

After the oxidation, both of the samples showed very bright background. In sample 1508, large amount of bright spots around the markers has been found. They are not SiV or NV, and will bleach away very fast once been focused on.

I couldn't re-find any marker from sample 1509 due to the large amount of fluorescence from the surface. For sample 1508, the region of interest next to marker 3C was still visible, despite all the disturbing bright spot next to it.

Sample 1509(substrate 207) was then acid cleaned, at the same time sample 1508 was moved into the cryostat, time resolved spectra were recorded. After the oxidation, we learned that the beam polarisation is not conserved within the photonic fibre, so that a polarising beam splitter and a liquid crystal noise eater was added after the fibre to obtain steadily vertically polarised beam. Using the same method as before oxidation, time-resolved PL spectra was recorded.

### 3.1.2 second Oxidation

The surface function groups play very important role regarding the surface charging state. It is interested to observe, the spectral behaviour of SiV in nanodiamonds, when the surface is initialized the same as bulk diamond. As reported in [Wolcott 2014], after 2 hours of aerobatic oxidation at  $575^{\circ}\text{C}$ , the surface structure of HPHT NDs is very similar to bulk single

crystals where hydroxyl and possibly ethers are the dominant functional groups. It is also interesting, since the elevated oxidation temperature can reduce the size of nanodiamond, to observe the behaviour change as the SiVs will be even closer to the surface after oxidation. Sample 1510 was prepared for this treatment, nanodiamond from batch1 was spin coated on the substrate186\_1 with method IV.

We tried to spin coat substrate 207 at the same time, but failed. The droplet of liquid refuse to spread over the surface while spinning, we suspect the surface of substrate has been damaged in our last oxidation session, which may result in a higher surface roughness that leads to poor wettability.

Taking the experiences of last oxidation into consideration. This time we introduced inert gas (helium) flow to flush away the potential contaminations during the cooling process. This can also prevent the result to be affected by the humidity of the air. We found out the extinction rate of polarising beam spliter was not ideal for 532nm, so this time we used a Clan Thompson polarisation filter instead.

As mentioned, the polarisation of the beam was not fixed in the measurement before the first oxidation, and while comparing the before and after oxidation spectra, we noticed that, even when the 2 sets of spectra are from the same poi, the spectra pattern can be very different. This made me wonder, if the polarisation of excitation beam has anything to do with the spectral diffusion. To figure this out, we measured the time-resolved PL spectra on 3 pois with different excitation beam polarisation at 4.7K.

The excitation polarisation pattern of other pois are also recorded, but due to low time and Helium budget, it was not affordable to record time resolved excitation polarisation for each of them. Time-resolved PL was later recorded at 20K.

After the oxidation, it was noticed that the sample looks much cleaner than last time. The confocal observation confirmed that, no bright dots like the ones from sample1508 has been seen. The increase of background fluorescence was observed again. Cold spectra showed the existence of GR1 center everywhere.

I noticed the intensity of GR1 fluorescence is stronger around the FIB made markers. As GR1 centre is a isolated vacancy inside diamond, it is reasonable to suspect that, the impact of focused ion beam may have caused serial collision and collision-induced dislocation inside diamond, resulting in the formation of GR1 centre. The fact that the intensity of GR1 centre is higher after the oxidation can also be explained by this theory, since the cross section is usually of the shape of a droplet, which is larger a few nm beneath the surface than on the surface.

## 3.2 H termination

As we discussed before, the origin of the band bending is that, the chemical potential of the surface and the bulk region need to match each other, while this adjustment changes the density of charges inside the diamond, it stimulates the generation of space charge, which need to be compensated by the surface charge that is compatible with the shift of the Fermi level from

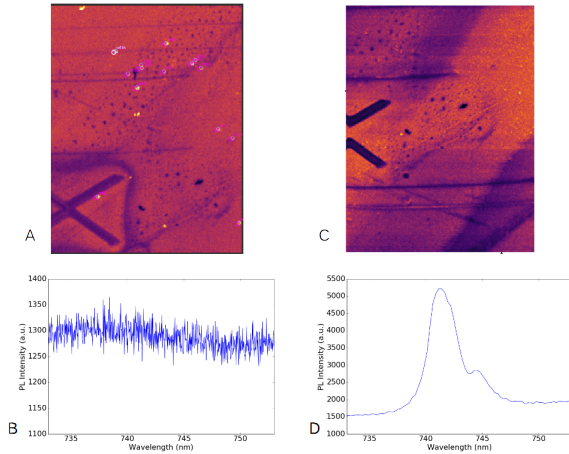


FIGURE 3.4: A: roi before oxidation, pois are mapped. B:Background spectrum of the region, no strong Gr1. C:roi after oxidation, strong background fluorescence, can't find pois. D:Spectrum after oxidation, strong GR1 center everywhere.

the charge neutrality level (CNL) of the surface state system. The hydrogenation of the diamond surface covers the surface with an atomic layer of  $C^-H^+$  dipole, which lead to a surface conducting band that is higher than the vacuum level, switches the surface from PEA to NEA.

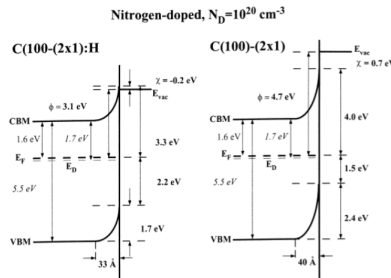


FIGURE 3.5: Band structure of N-doped diamond, due to the shift of surface chemical potential, Hydrogenated diamond has flatter band bending than dehydrogenated diamond.Diederich et al., 1998

The surface termination is carried out in a microwave plasma reactor. This is operated by Dr. Christian Osterkamp. The parameters are: Hydrogen flow: 300sccm, temperature: 750°C. The duration of the treatment was 3.5min. In Yeap, Chen, and Loh, 2009, the reaction lasted 60min to maximize the coverage, in our case, considering the low density of nanodiamond on the substrate, we applied the same amount of time as bulk diamond, as the nanodiamond can already be 'dipped' into the plasma thoroughly. The sample that has been used is sample 1512. Sample 1512

was produced by spin coating nanodiamond batch1 on the substrate 186\_2, with method IV.

To prevent introducing contamination into the plasma reactor, no characterisation has been done before the termination. The plasma reactor has the similar vacuum system as a conventional electron microscope, the sample was first put into a pre-vacuum chamber then send into the reaction chamber. The shape of the plasma is controlled by a quartz waveguide.

After the termination, we put the sample directly into the cryostat, very high density of SiV has been found and marked. It has been recorded as before, the excitation polarisation pattern and the time-resolved PL spectra.

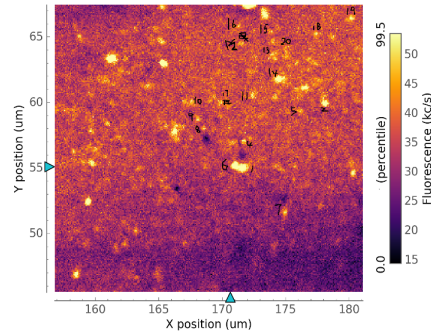


FIGURE 3.6: Very high density of SiV has been found in sample 1512



## Chapter 4

# Result and Discussion

### 4.1 Compilation of data

To investigate the spectral diffusion behaviour, recorded time-resolved spectra for each of the POI before and after treatment. After the first oxidation, for better characterisation, time-resolved spectra are measured not only with one but multiple excitation polarisation. This leaves large amount of spectra files (almost 32,000 spectra!), besides visualizing the movement of lines into color maps, we need better tools to evaluate the spectral stability, a way to compile dozens, sometimes even hundreds of spectra into one single value that represents the spectral stability of a POI.

Normalized cross-correlation evaluates the similarity between 2 patterns, the closer to 1, the higher the similarity. Here we compare the time-resolved PL spectra from every time tick with the first spectrum, the average value of this series of normalized cross-correlation reflects the general level of spectral stability of the measured point.

### 4.2 Nanodiamond size and spectral stability

The observation of nanodiamond with SEM [fig.] fits the expectation, that after the centrifuging size selection, batch1 contains smaller nanodiamonds than batch2. When comparing the time-resolved spectra from sample1508 and sample1510, which were taken at 4K, with an excitation power of  $120 \pm 10 \mu\text{W}$ , it can be observed that the spectra from sample1510 shows more spectral diffusion. The calculation of mean normalized cross-correlation confirmed the observation. As plotted in the histogram 4.7, the distribution of mean normalized cross-correlation nanodiamond from batch1 is much closer to 1 than from nanodiamond batch2.

As discussed in Chapter 1, in nitrogen doped diamond, to match up the chemical potential inside the diamond and on the surface, a depletion layer was formed beneath the surface, where the valence band and conducting band are bended towards up. The width of the depletion layer differs by the concentration of the donor and is around 80nm in moderately doped diamond ( $N_D = 10^{-16}/\text{cm}^3$ ) Diederich et al., 1998

Since the donor level of nitrogen is rather deep (1.7eV) below the minimum of conduction band, it is very hard to thermally ionize the donors at low temperature, but with the excitation of 532nm(2.33eV) green laser, it is possible to excite the electrons from the donor level to the conduction band.

So in our case, there is higher chance for nanodiamonds from batch1, which are of smaller sizes, to obtain  $\text{SiV}^-$ 's sitting inside the bended band

than those ones of larger diameters, like the ones from batch2. For more information I looked up the position of SiV<sup>-</sup>s in the paper Rogers et al., 2013, where SiV<sup>-</sup>s in bulk diamond are reported to have very good long term spectral stability (no spectral position variation in 90min), interestingly, the distance of SiV<sup>-</sup>s from the surface is larger than 2um, which means they sat in the bulk diamond region instead of band bended region.

### 4.3 Excitation power and spectral stability

Sample 1508 was excited with decreasing excitation power. The left column of 4.6 shows the changes of time-resolved spectra of POI ref11, the most obviously diffusing line is the one between 738nm and 739nm, whose spectral position changed almost 1nm in 300s. As the excitation power decreases, the diffusion become less intense.

The result of cross correlation is can be seen in 4.1, where each dot represents a POI in the sample. As shown in the figure, the general level of spectral diffusion decreases as the excitation power decreases.

A possible reason for this behaviour is the optical transition between the Nitrogen donor level and the conduction band has been involved in the excitation of SiV<sup>-</sup>. The nitrogen donor level lies 1.7eV below the minimum of diamond conduction band Diederich et al., 1998, the spontaneous emission between the valence band and the donor level is capable of excite the SiV<sup>-</sup> from ground state to the first excited state.

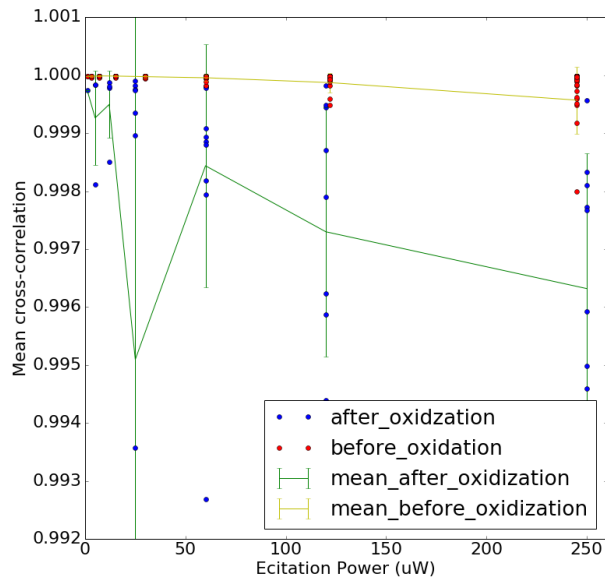


FIGURE 4.1: Powerdependency of nanodiamond batch2, before and after first oxidation.

## 4.4 Temperature and spectral stability

Comparing the mean normalized cross-correlation of sample 1510 from 4.7K and 20K in 4.7, no significant difference between the two temperatures has been found, which fits the expectation. Since the assumption is that, the donors are ionized with the help of laser, the band bending should stay the same as long as the excitation power is not changed, so shall the spectral diffusion. I consider this result not solid enough as only 3 points were measured for the 4.7K measurement. But it would be interesting to collect more data to justify the prediction.

## 4.5 Excitation polarisation and spectral stability

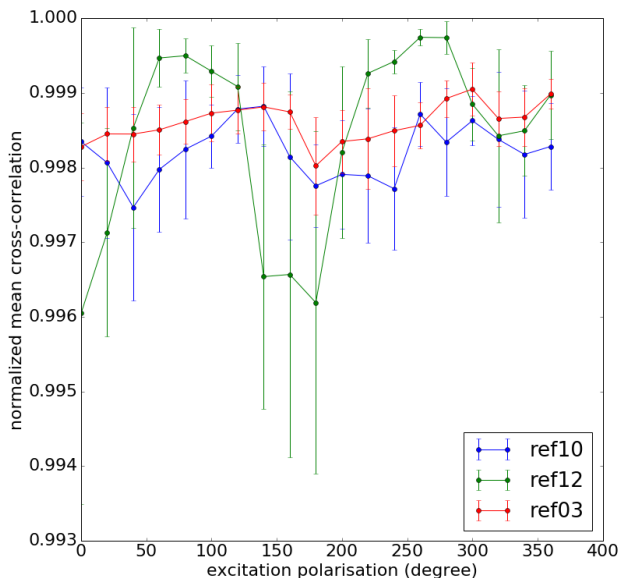


FIGURE 4.2: Mean normalized cross-correlation against excitation polarisation. The error bar stand for standard deviation

The polarisation of photoluminescence has been measured in Rogers et al., 2014a, where the excitation polarisation patterns suggested that the SiV<sup>-</sup> is aligned along the <111> axis of diamond crystal. A set of dots of none-polarisation dependency(excite from the z axis of the SiV<sup>-</sup>), or symmetric patterns that are rotationally separate from each other by an angle of 60° with population contrast of 60% are expected to be observed when excite the SiV<sup>-</sup> along crystal axis <111>. The polarisation pattern generated from other orientations can be considered as shadowing the <111> axis from respective angle.

In the measurement of excitation polarisation on sample 1510, time-resolved PL spectra are taken with different excitation polarisations. We do noticed some POIs behaved differently when excited with different beam

polarisation<sup>4.4</sup>. But no clear polarisation pattern has been acquired. Further cross-correlation calculation <sup>4.2</sup> showed polarisation dependency like pattern in poi ref12, while the other two pois have no clear pattern.

Further excitation polarisation-resolved spectra were taken on the same sample. In some of the spectra, polarisation-related periodic pattern can be seen on some of the lines, while the sum up pattern give no polarisation dependency.

## 4.6 Aerobic Oxidation and Spectral stability

The initial target for aerobic oxidation is to selectively remove graphitic defects(the first oxidation) and to generate bulk diamond-like surfaces(the second oxidation). The second oxidation, which was operated on sample 1510, didn't turn out as we wished, offering no useful data on SiV<sup>-</sup>. The first oxidation on sample1508 and 1509 introduced dark spots that are visible in optical microscopy images, and very bright spots containing no SiV<sup>-</sup> signal in confocal measurements. These are suspected to be exotic, as the furnace has been used for other materials. Yet it was managed to re-find some of the pois from sample1508.

The aerobic oxidation has greatly enhanced the photoluminescence of the sample in general, including SiV<sup>-</sup> and background. The left column of <sup>4.11</sup> shows the comparison of spectrometer recorded intensity between before and after oxidation, as can be seen in ref3 and other points, the magnification of the enhancement is not uniform. The broadening of peak is also observed. The number of peaks that are distinguishable has decreased after the oxidation. While the spectra before oxidation consists of multiple thinner peaks, the spectra after oxidation contains broader peaks joining with each other. It is suspected that the spectrometer was not well aligned, which results in the broadening of peak and the disappearance of fine structure. Despite the broadening, an visible enhancement <sup>4.12</sup> in the spectral diffusion was also noticed, mean cross-correlation comparison can be found in <sup>4.10</sup>. The power dependency of spectral diffusion (mean cross-correlation) is plotted in <sup>4.1</sup>, with similar trend as before oxidation: the spectral diffusion increases as excitation power increases. The drop of 30uW is due to an extreme point which obtained very noisy background, that is related to the suspected exotic luminescence from the oxidation process.

## 4.7 Hydrogen termination and Spectral stability

Hydrogen terminated diamond surface posses negative electron affinity (Maier, Ristein, and Ley, <sup>2001</sup>; Ristein, <sup>2000</sup>; Diederich et al., <sup>1998</sup>) and is related to the depletion of NV centres in diamond (Stacey et al., <sup>2012</sup>). After hydrogen plasma treatment on sample1512(nanodiamonds batch1) as mentioned in ??, time-resolved PL and excitation polarisation-resolved PL were recorded at 20K.

The time resolved pattern has been plotted out in <sup>4.13</sup>, a visibly improvement in the spectral stability is shown. The comparison of mean cross-correlation of untreated nanodiamonds batch1 and hydrogenated ones can be found in <sup>4.8</sup>, which agrees with the observation. As reference the comparison between nanodiamonds batch2 and hydrogen terminated batch1

was also plotted 4.9. The hydrogenated nanodiamonds also responds the changes in excitation polarisation better. Clear polarisation dependency pattern can be seen in 4.14. It has been noticed in the polarisation pattern of untreated nanodiamonds, that despite the general pattern reflects no polarisation dependency, some of the lines can still be seen changing periodically with the excitation polarisation. If we look closely at figure B and E in 4.14, between 735nm and 737nm, there is a broader and less bright band whose not only intensity but also width changes with excitation polarisation. This pattern has also been seen in the pre-treatment sample.

## 4.8 Discussion

The size effect of colour centre in nanodiamonds is often related to the surface band bending phenomena. The larger the diamond, the less effect from the band bending have on the whole diamond.

As the samples are nitrogen doped, it is expected to have a upward band-bending, with a fermi level between the conduction band and the donor level. When the surface chemical potential is low enough, it is possible to have the donor level, even valence band maximum of the bulk region crossing the fermi level near the surface, which results in the accumulation of holes.

The Nitrogen atom level lies 1.7eV below the minimum of the conduction band (Diederich et al., 1998), at cryogenic temperature, the main electron source is the photon-excited electrons, with our 532nm excitation laser, it is not possible to excite electron from the valence band, but possible from the donor level.

Since the accumulation of holes at the nitrogen atom level, the electrons from the conduction band are encouraged to recombine with the holes and emit photons. Since 1.7eV is already larger than the band gap between SiV<sup>-</sup> ground state and the first excited state, these spontaneous emission can be involved in the excitation of SiV<sup>-</sup>s. While the polarisation of spontaneous emission is not relevant to the excitation polarisation, the excitation polarisation pattern of SiV<sup>-</sup> may not be solely the reflection of excitation polarisation but also the polarisation of spontaneous emission from the conduction band, which explains the patterns in 4.3.

As excitation power increases, more electrons are excited into the conduction band, which leads to further increase of spontaneous emission, which can be related to the power dependency of spectral diffusion in 4.1 and 4.6 that the spectral diffusion reduces as the power decreases.

It is assumed that the surface treatment alters the surface chemical potential and affects the depth of the hole accumulating region. In (Stacey et al., 2012) it is mentioned that the hydrogenation induced larger upward band bending in diamonds, while in (Diederich et al., 1998) the hydrogenated n-doped diamond had smaller upward band bending than the 'clean' one. This is because, the low surface potential in (Stacey et al., 2012) is caused by adsorbent (water layer), while (Diederich et al., 1998) discussed adsorbent-free surfaces. Our sample is measured in UHV at cryogenic temperature, there shall be no water layer or other surface adsorbent involves, so we assume a reduced band bending is formed under the surface after hydrogenation, and this fits the measurement result.

From the result it seems the aerobic oxidation has decreased the surface potential, which increases the

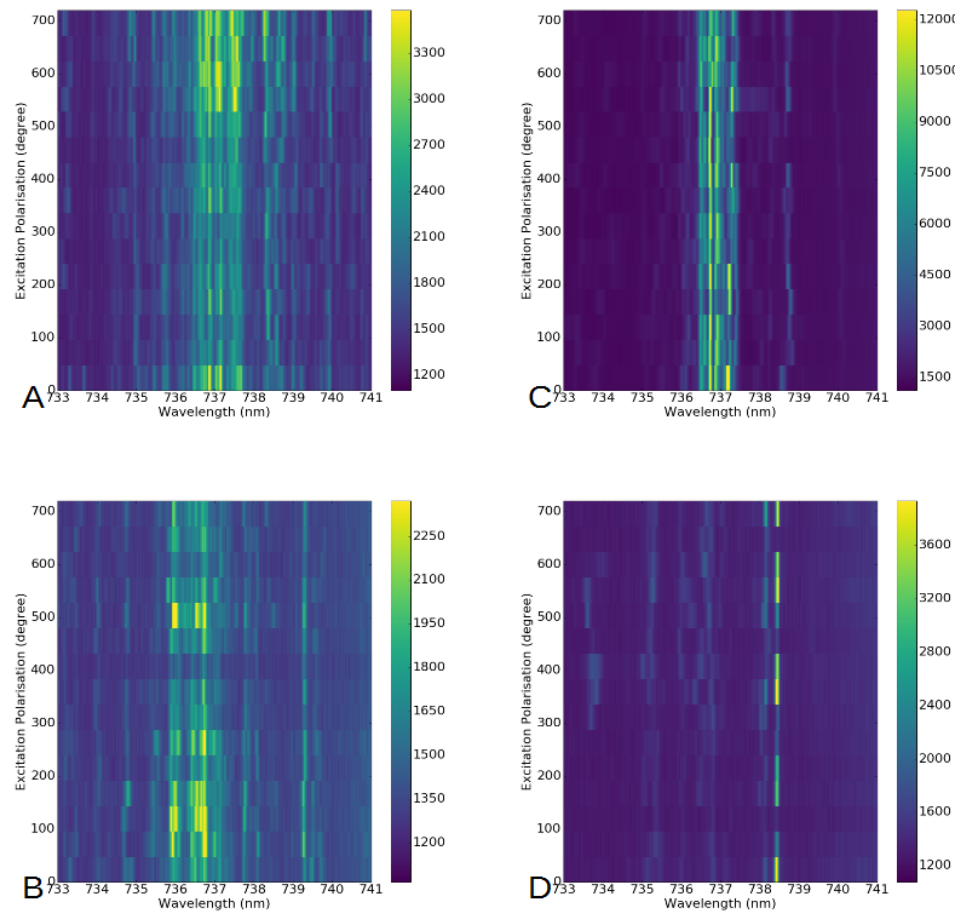


FIGURE 4.3: 4 Excitation polarisation-resolved spectra from sample 1510, A: ref16, B:ref13, C:ref15, D:ref12. Some of the lines in these spectra show polarisation dependency, most significantly can be seen in ref12

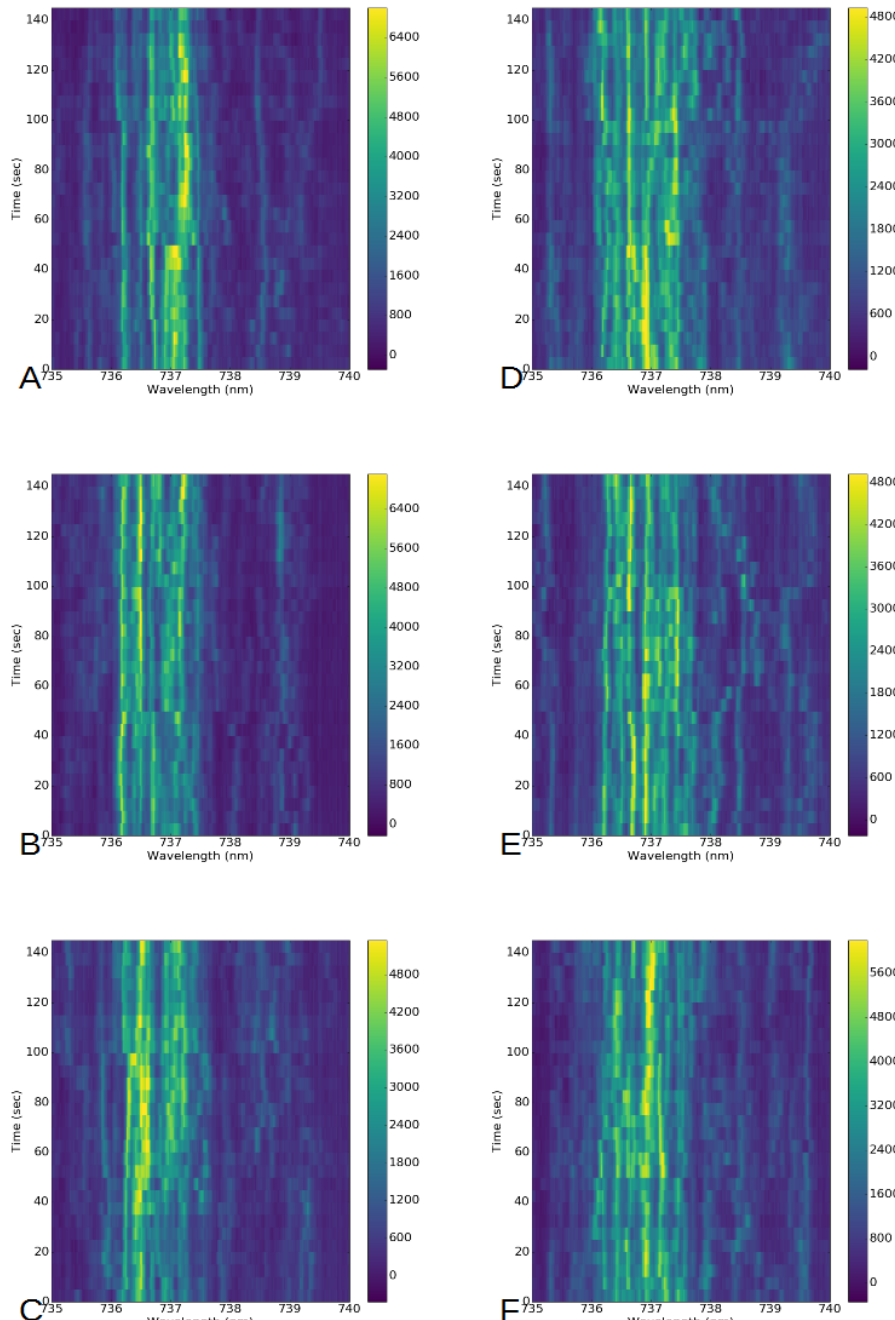


FIGURE 4.4: Time-resolved spectra of poi ref03, sample1510 with different excitation polarisation. Polarisation of the excitation beam: A:  $0^\circ$ , B:  $40^\circ$ , C:  $80^\circ$ , D:  $120^\circ$ , E:  $160^\circ$ , F:  $200^\circ$ .

This figure continues in 4.5

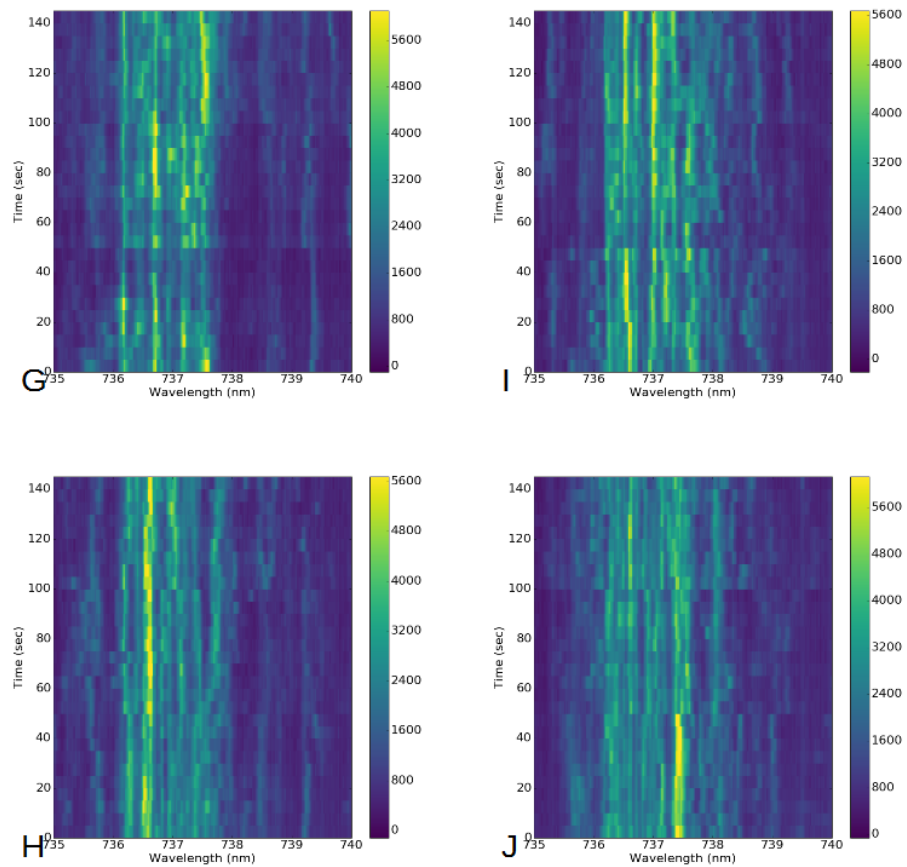


FIGURE 4.5: This figure follows 4.4. Excitation Polarisation:  
 G:  $240^\circ$ , H:  $280^\circ$ , I:  $320^\circ$ , J:  $360^\circ$

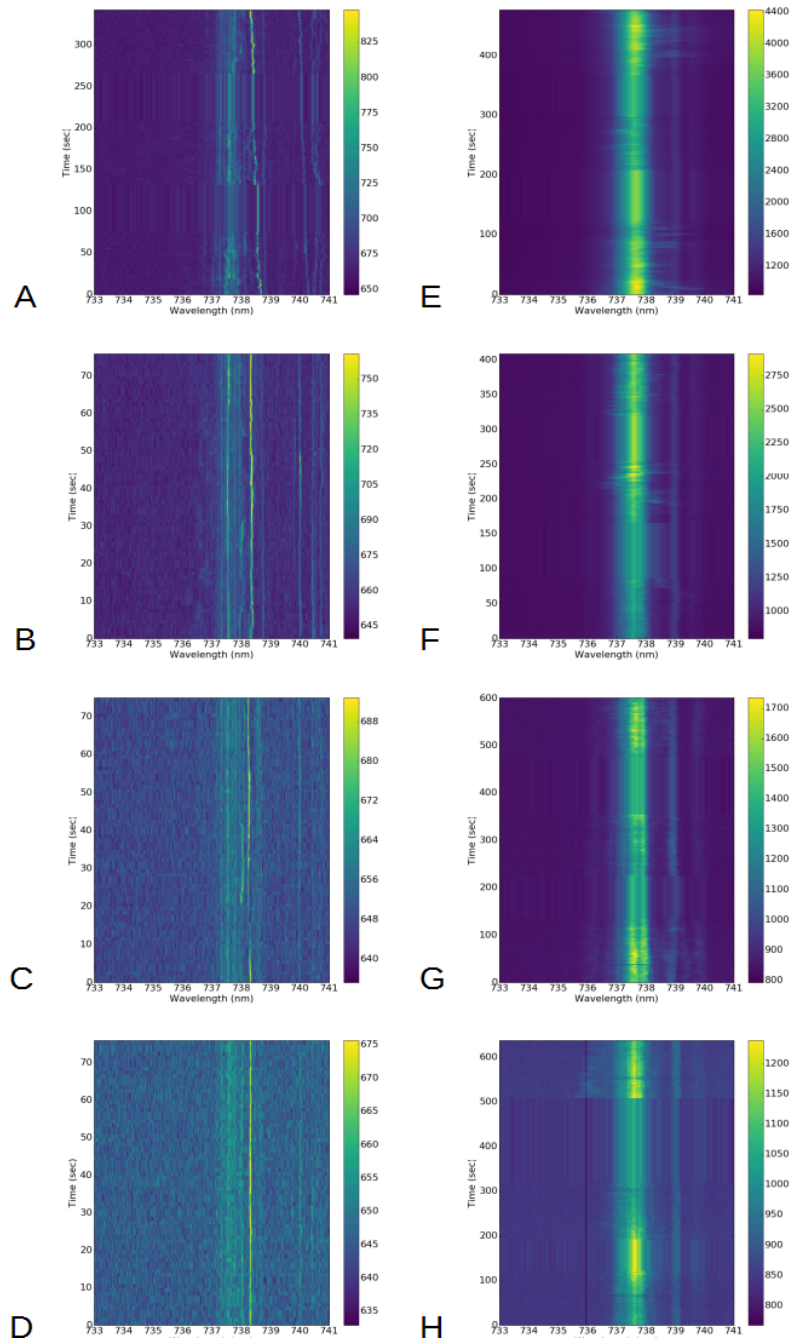


FIGURE 4.6: Left column: time resolved PL spectra of point ref11, sample1508 before the first aerobic oxidation with different excitation power (A:250uW, B:122uW, C:60uW, D:30uW). Right column:time resolved PL spectra of point ref11, sample1508 after the first aerobic oxidation with different excitation power (A:250uW, B:120uW, C:60uW, D:25uW). The spectra were plotted in the order of real time, the stretched pixel is the blank for refocus.

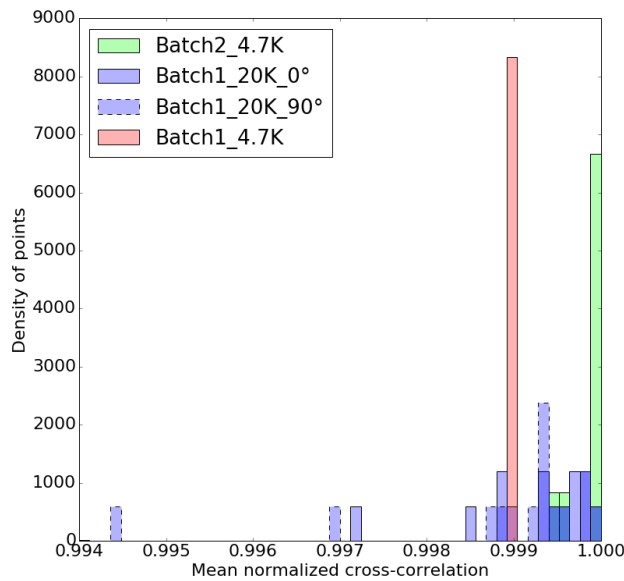


FIGURE 4.7: Histogram comparing the normalized mean value of cross-correlation between untreated sample 1508 (nanodiamond batch2) at 4.7K and sample 1510(nanodiamond batch1) at 4.7K and 20K. The height of the bars are normalized by the integration over bins. The time resolved spectra of sample 1510 was recorded with 2 different excitation polarisation, they are separated with solid and dashed lines.

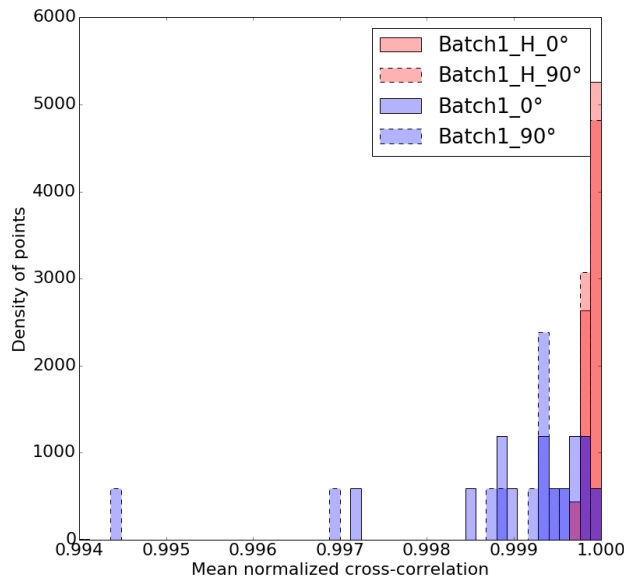


FIGURE 4.8: Histogram comparing the normalized mean value of cross-correlation between untreated sample 1510 and hydrogen plasma treated sample 1512 (both spin coated with nanodiamond from the batch1).The height of the bars are normalized by the integration over bins.

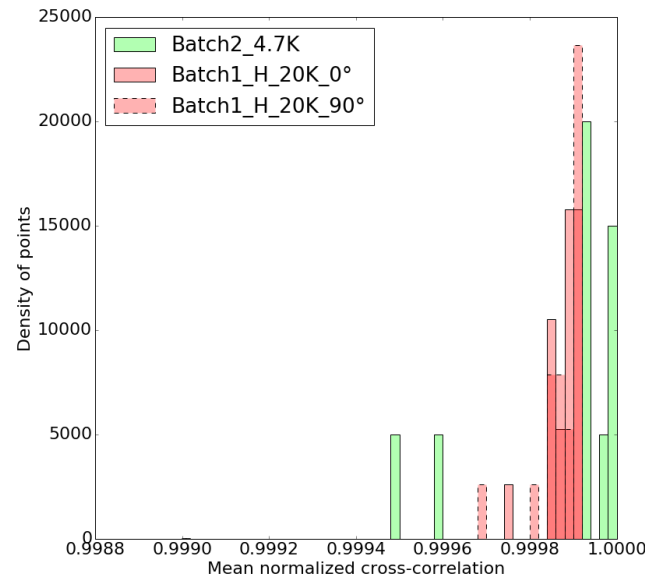


FIGURE 4.9: Histogram comparing the normalized mean value of cross-correlation between untreated sample 1508(nanodiamond batch2) and hydrogen plasma treated sample 1512(nanodiamond batch1).The height of the bars are normalized by the integration over bins.

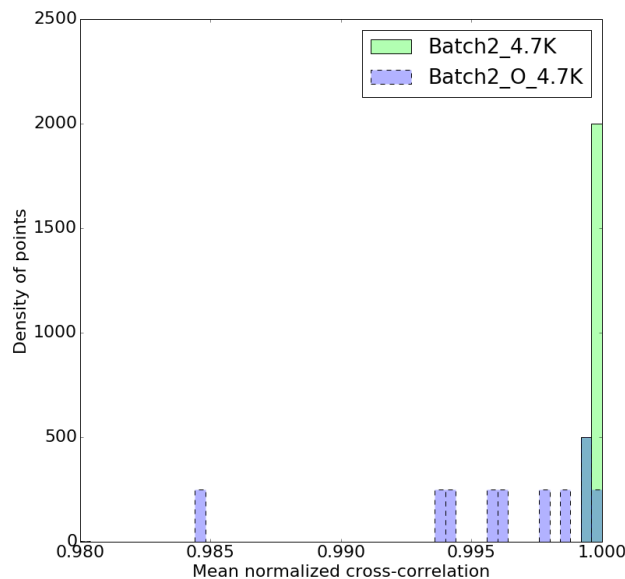


FIGURE 4.10: Histogram comparing the normalized mean value of cross-correlation between untreated and oxidized sample 1509(nanodiamond batch1) at 4.7K. The height of the bars are normalized by the integration over bins.

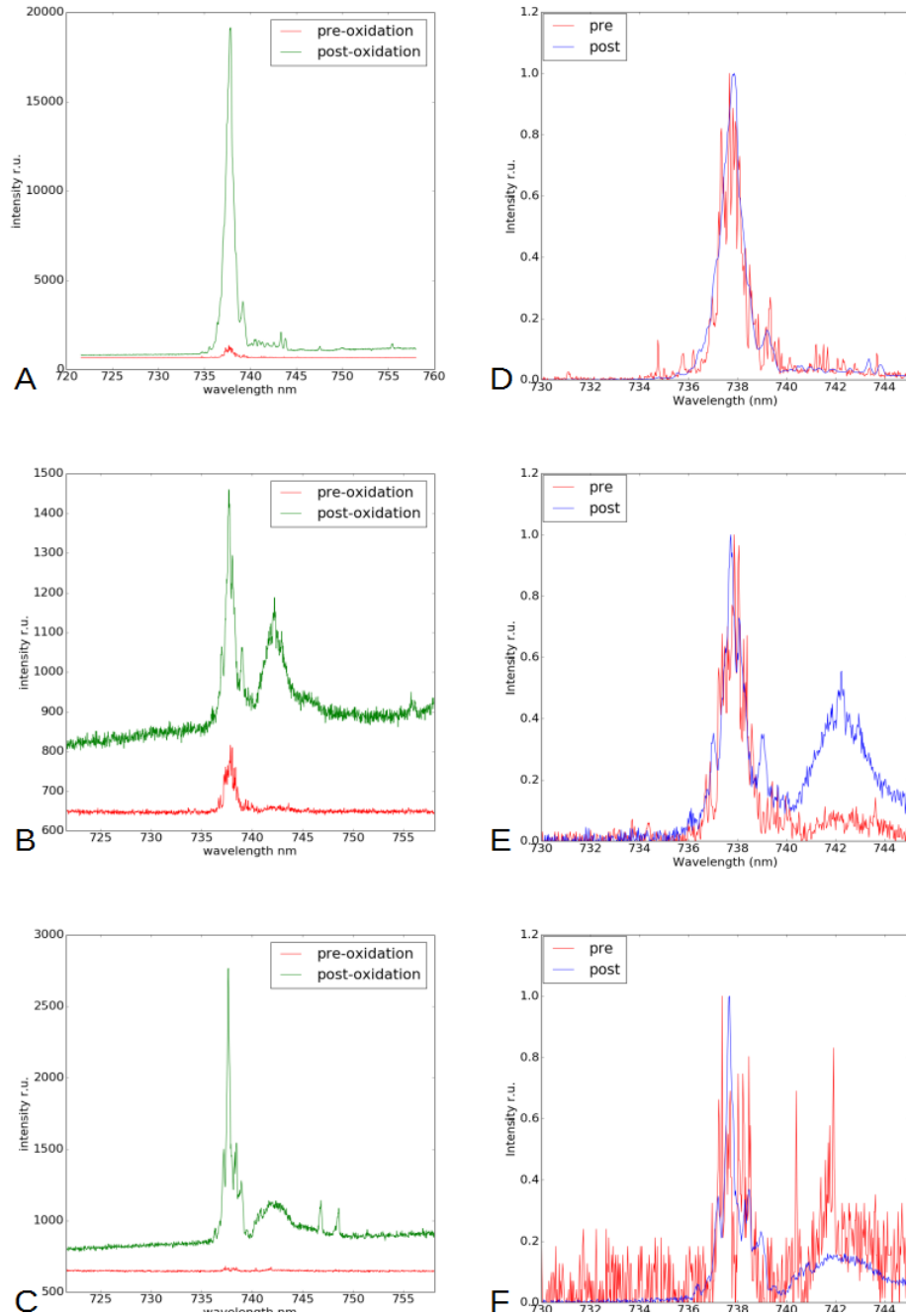


FIGURE 4.11: Comparison between the PL Spectra of 3 of the pois from sample1508. Left column: real value. Right column: normalized spectra. The spectra were recorded with 120uW of excitation power with 532nm green laser and 1s of exposure time. A,D: ref4, B,E: ref3, C,F: ref5.

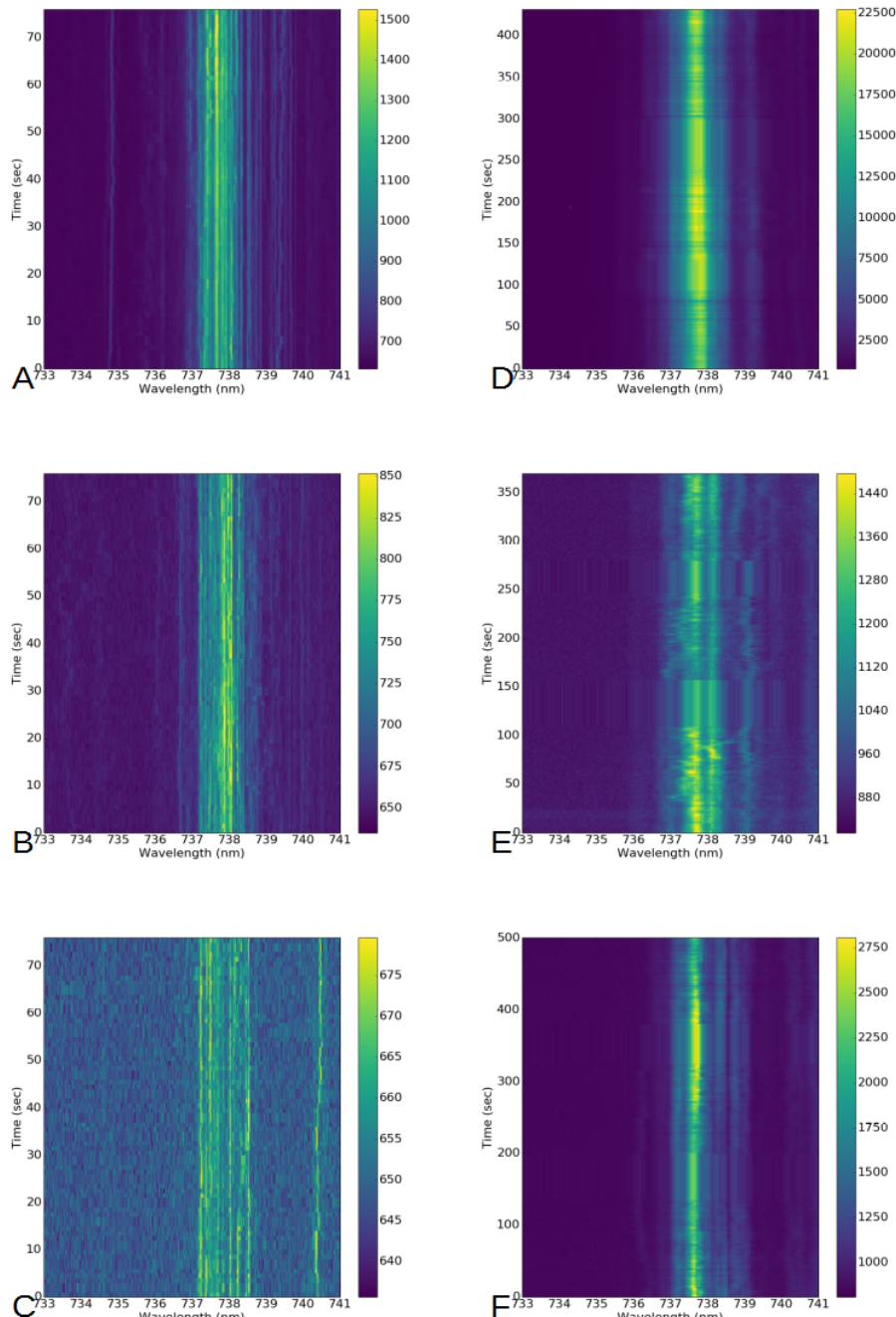


FIGURE 4.12: The time-resolved spectra of pois from 4.11. The spectra were also recorded with 120uW of excitation power with 532nm green laser and 1s of exposure time. Left column: before oxidation, right column: after oxidation. A,D: ref4, B,E: ref3, C,F: ref5. The spectra were plotted in the order of real time, the stretched pixel is the blank for refocus.

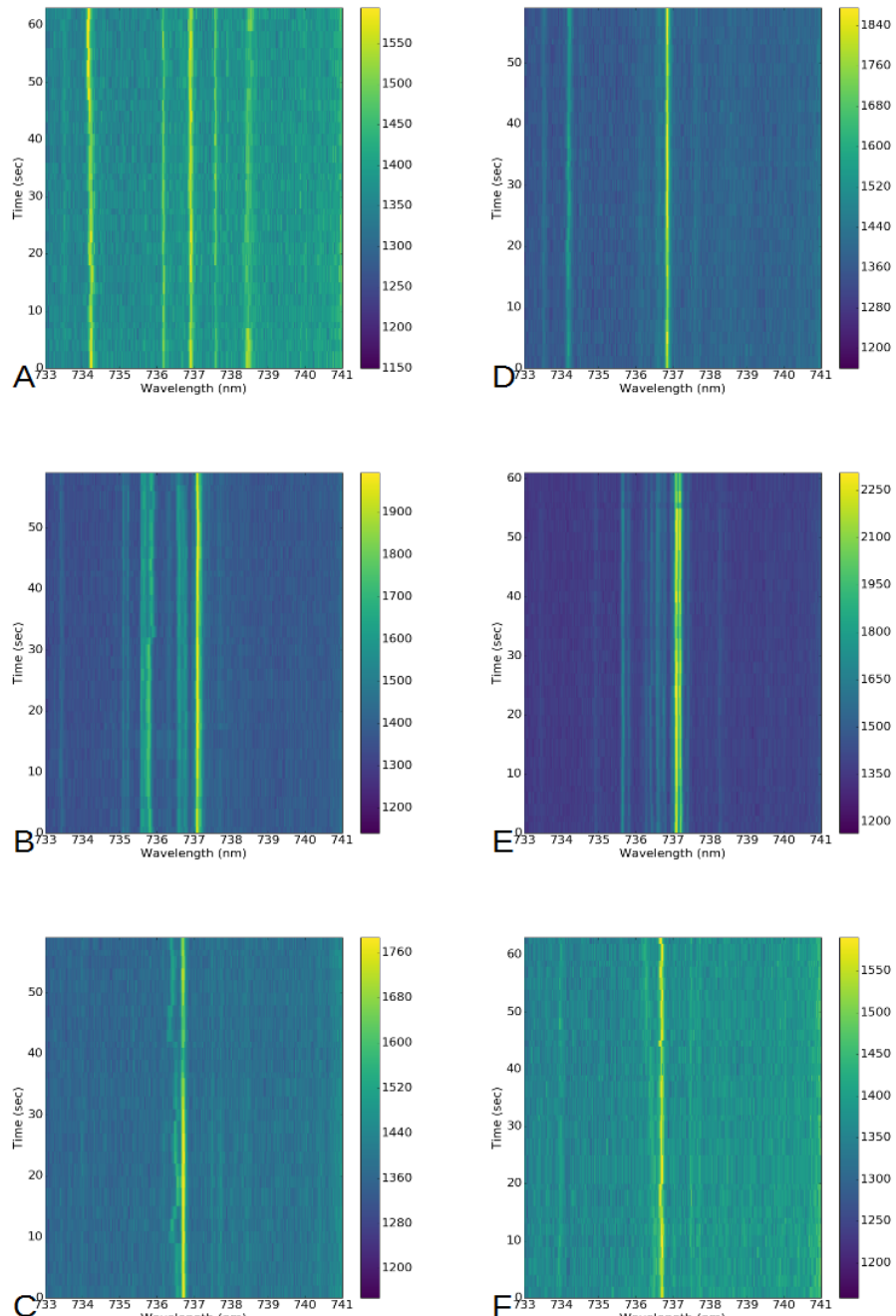


FIGURE 4.13: Time-resolved PL spectra of poi ref18, ref19 and ref20 from sample1512 at 20K. The excitation polarisation of left and right column are perpendicular to each other. A,D: ref20, B,E: ref19, C,F: ref18

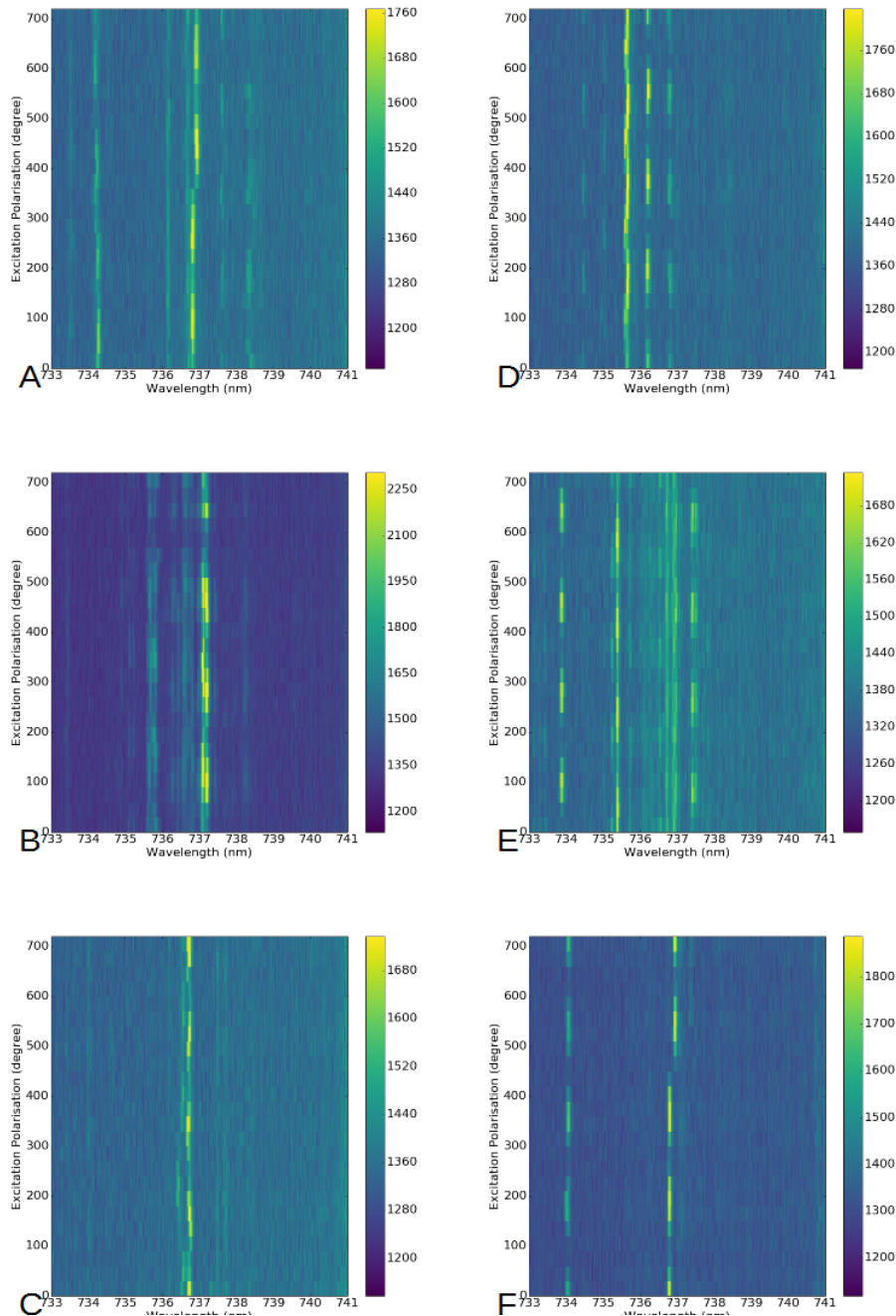


FIGURE 4.14: The excitation polarisation-resolved spectra of pois from sample1512 at 20K. A: ref20, b:ref19, C:ref18, D:ref15, E:ref13, F:ref12.

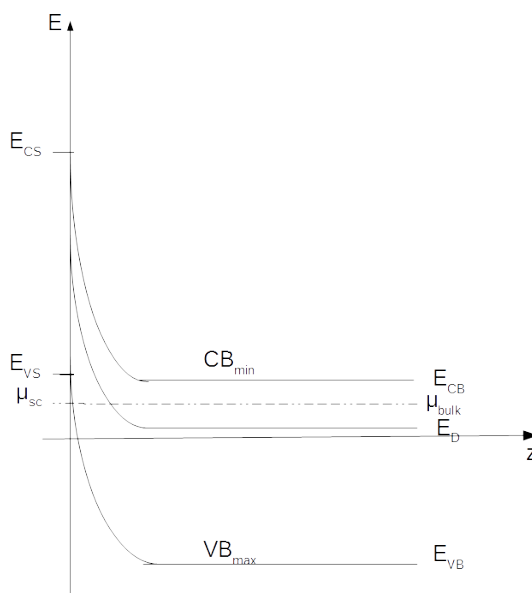


FIGURE 4.15: Sketch of band bending in n doped nitrogen vacancy. The cross over of fermi level and nitrogen atom level may cause the accumulation of holes.  $E_D$ : donor level, the nitrogen atom level.  $E_{CB}$ : bulk conduction band minimum.  $E_{VB}$ : bulk valence band maximum.  $E_{CS}$ : surface conduction band minimum.  $E_{VS}$ : surface valence band maximum.  $\mu_{SC}$ : surface chemical potential.  $\mu_{bulk}$ : bulk chemical potential.



# Chapter 5

## Conclusion and outlook

### 5.1 Conclusion

In the thesis we characterised spectrally the SiV<sup>-</sup> in nanodiamonds of 2 different size distributions with the help of confocal microscopy at cryogenic temperature. It has been noticed that the untreated SiV<sup>-</sup> in nanodiamonds are spectrally not stable, and SiV<sup>-</sup> smaller diamonds have worse spectral stability than larger ones. This spectral diffusion can be resolved in PL spectra. Previously it has been shown that the surface charging state plays a vital role in color centre luminescence. Negative charges on the surface can lead to depletion of NV (Stacey et al., 2012). For nanodiamonds, the band bending which originates from the difference of chemical potential in the bulk and on the surface is closely related to size-effect relating phenomena. It is highly suspected that the spectral diffusion of SiV<sup>-</sup> in nanodiamonds is also surface charge related.

Large number of PL spectra were taken to trace drift of lines. A standard method for spectral stability has been put forward. The calculation of mean cross-correlation can conclude the similarity of spectra into one number ranging from 0 to 1, Which makes statistical comparison possible. At the same time, time-resolved spectra realises the visualisation of spectra diffusion by plotting spectra over time in to colour maps.

Three surface treatment has been employed to modify the surface charging property. Aerobic Oxidation at 460°C - 480°C was used to selectively remove the graphitic defects on the surface while mild oxidation, resulting in carbonyl and carboxyl groups covered surface. Elevated temperature oxidation (575°C) was used to initialize a bulk-diamond-like surface structure. Hydrogenation was to form a surface that posses negative electron affinity.

The oxidation at elevated temperature didn't produce useful data due to the distraction of substrate. The mildly oxidized sample showed heavily enhanced luminescence and worse spectral stability while the hydrogen terminated sample showed slightly reduced luminescence intensity and improved spectral stability.

### 5.2 Outlook

**PL and PLE** It is suspected that the ionization of Nitrogen atoms has been involved in the process, it is interested to compare the time-resolved spectra excited with a 532nm laser and a laser of 730nm.

PLE characterisation of the sample with improved spectra stability is also attractive, with reduced spectral diffusion, it might be finally possible for us to resolve the 4 line structure of SiV<sup>-</sup> ZPL.

**life time measurement** Due to the spectral diffusion, the orbital T1 measurement of untreated sample was not able to be carried out. With the improved spectral stability (need to be proved by PLE first), it might become possible. A longer time life will offers more possibility on the development of SiV<sup>-</sup> qubit.

**Surface treatments** Different surface treatments and comparison can help us understand the mechanism of spectral diffusion better. The most convenient treatments now are the hydroxylation which can be carried out directly on the hydrogenated sample resulting in a transform from negative electron affinity to positive electron affinity of the surface.

Anther interesting treatment is the dehydrogenation of sample by vacuum annealing, as the temperature varies, this can result in a clean diamond surface or a surface covered with thin-thick layer of graphite, which results in a gradual change in the surface electron affinity. (Diederich et al., 1998; Maier, Ristein, and Ley, 2001)

Aerobic Oxidation still has more possibility to deal with. Since the size reduction rate of certain temperature is known, it is possible to profile the size effect on spectral stability by decreasing the size of nanodiamonds via oxidation gradually. It can also used to treat nanodiamonds that are too large (batch3, 4) for phonon elimination. The oxidation can also help to separate aggregated diamonds.

**better method for size selection** It is noticed, the size selection via centrifugation works, but is quite coarse. It might be possible to obtain finer batches by methods like high performance liquid chromatography. (Naoki Komatsu, 2011)

**relation between surface geometry and spectral behaviour** Since it is possible to obtain the excitation polarisation pattern, it is interesting to observe the orientation preference of SiV<sup>-</sup>/nanodiamonds statistically. This can be related to the formation process of HPHT diamond.

## Appendix A

### Appendix Title Here

Write your Appendix content here.



# Bibliography

- Albrecht, A. et al. (2013). "Coupling of nitrogen vacancy centres in nanodiamonds by means of phonons". en. In: *New Journal of Physics* 15.8, p. 083014. ISSN: 1367-2630. DOI: [10.1088/1367-2630/15/8/083014](https://doi.org/10.1088/1367-2630/15/8/083014). URL: <http://stacks.iop.org/1367-2630/15/i=8/a=083014> (visited on 10/11/2016).
- Bassett, L. C. et al. (2014). "Ultrafast optical control of orbital and spin dynamics in a solid-state defect". en. In: *Science* 345.6202, pp. 1333–1337. ISSN: 0036-8075, 1095-9203. DOI: [10.1126/science.1255541](https://doi.org/10.1126/science.1255541). URL: <http://www.sciencemag.org/cgi/doi/10.1126/science.1255541> (visited on 10/10/2016).
- Buckley, B. B. et al. (2010). "Spin-Light Coherence for Single-Spin Measurement and Control in Diamond". en. In: *Science* 330.6008, pp. 1212–1215. ISSN: 0036-8075, 1095-9203. DOI: [10.1126/science.1196436](https://doi.org/10.1126/science.1196436). URL: <http://www.sciencemag.org/cgi/doi/10.1126/science.1196436> (visited on 10/10/2016).
- Childress, Lilian, Ronald Walsworth, and Mikhail Lukin (2014). "Atom-like crystal defects: From quantum computers to biological sensors". en. In: *Physics Today* 67.10, pp. 38–43. ISSN: 0031-9228, 1945-0699. DOI: [10.1063/PT.3.2549](https://doi.org/10.1063/PT.3.2549). URL: <http://scitation.aip.org/content/aip/magazine/physicstoday/article/67/10/10.1063/PT.3.2549> (visited on 10/10/2016).
- Clark, C. D. et al. (1995). "Silicon defects in diamond". In: *Physical Review B* 51.23, pp. 16681–16688. DOI: [10.1103/PhysRevB.51.16681](https://doi.org/10.1103/PhysRevB.51.16681). URL: <http://link.aps.org/doi/10.1103/PhysRevB.51.16681> (visited on 10/10/2016).
- Davydov, V. A. et al. (2014). "Production of nano- and microdiamonds with Si-V and N-V luminescent centers at high pressures in systems based on mixtures of hydrocarbon and fluorocarbon compounds". en. In: *JETP Letters* 99.10, pp. 585–589. ISSN: 0021-3640, 1090-6487. DOI: [10.1134/S002136401410004X](https://doi.org/10.1134/S002136401410004X). URL: <http://link.springer.com/10.1134/S002136401410004X> (visited on 06/01/2016).
- Diederich, L. et al. (1998). "Electron affinity and work function of differently oriented and doped diamond surfaces determined by photoelectron spectroscopy". In: *Surface Science* 418.1, pp. 219–239. ISSN: 0039-6028. DOI: [10.1016/S0039-6028\(98\)00718-3](https://doi.org/10.1016/S0039-6028(98)00718-3). URL: <http://www.sciencedirect.com/science/article/pii/S0039602898007183> (visited on 10/10/2016).
- Dietrich, Andreas et al. (2014). "Isotopically varying spectral features of silicon-vacancy in diamond". In: *New Journal of Physics* 16.11, p. 113019. ISSN: 1367-2630. DOI: [10.1088/1367-2630/16/11/113019](https://doi.org/10.1088/1367-2630/16/11/113019). URL: <http://stacks.iop.org/1367-2630/16/i=11/a=113019?key=crossref.82aa49b97773b65bb6774d744bd5a404> (visited on 10/10/2016).

- DiVincenzo, David P. and IBM (2000). "The Physical Implementation of Quantum Computation". In: *Fortschritte der Physik* 48.9-11. arXiv: quant-ph/0002077, pp. 771–783. ISSN: 00158208, 15213978. DOI: 10.1002/1521-3978(200009)48:9/11<771::AID-PROP771>3.0.CO;2-E. URL: <http://arxiv.org/abs/quant-ph/0002077> (visited on 10/10/2016).
- Gali, Adam and Jeronimo R. Maze (2013). "\textit{Ab initio} study of the split silicon-vacancy defect in diamond: Electronic structure and related properties". In: *Physical Review B* 88.23, p. 235205. DOI: 10.1103/PhysRevB.88.235205. URL: <http://link.aps.org/doi/10.1103/PhysRevB.88.235205> (visited on 10/10/2016).
- Goss, J. P. et al. (1996). "The Twelve-Line 1.682 eV Luminescence Center in Diamond and the Vacancy-Silicon Complex". In: *Physical Review Letters* 77.14, pp. 3041–3044. DOI: 10.1103/PhysRevLett.77.3041. URL: <http://link.aps.org/doi/10.1103/PhysRevLett.77.3041> (visited on 10/10/2016).
- Iakoubovskii, K. and G. J. Adriaenssens (2000). "Luminescence excitation spectra in diamond". In: *Physical Review B* 61.15, pp. 10174–10182. DOI: 10.1103/PhysRevB.61.10174. URL: <http://link.aps.org/doi/10.1103/PhysRevB.61.10174> (visited on 10/11/2016).
- Inam, F. A. et al. (2011). "Modification of spontaneous emission from nanodiamond colour centres on a structured surface". en. In: *New Journal of Physics* 13.7, p. 073012. ISSN: 1367-2630. DOI: 10.1088/1367-2630/13/7/073012. URL: <http://stacks.iop.org/1367-2630/13/i=7/a=073012> (visited on 10/11/2016).
- Jantzen, Uwe (2015). "Low temperature spectroscopy of single colour centers in nanodiamonds". Diplom Thesis. Ulm University.
- Jantzen, Uwe et al. (2016). "Nanodiamonds carrying silicon-vacancy quantum emitters with almost lifetime-limited linewidths". en. In: *New Journal of Physics* 18.7, p. 073036. ISSN: 1367-2630. DOI: 10.1088/1367-2630/18/7/073036. URL: <http://stacks.iop.org/1367-2630/18/i=7/a=073036> (visited on 10/11/2016).
- Kleppner, Daniel (1981). "Inhibited Spontaneous Emission". In: *Physical Review Letters* 47.4, pp. 233–236. DOI: 10.1103/PhysRevLett.47.233. URL: <http://link.aps.org/doi/10.1103/PhysRevLett.47.233> (visited on 10/10/2016).
- Maier, F., J. Ristein, and L. Ley (2001). "Electron affinity of plasma-hydrogenated and chemically oxidized diamond (100) surfaces". In: *Physical Review B* 64.16, p. 165411. DOI: 10.1103/PhysRevB.64.165411. URL: <http://link.aps.org/doi/10.1103/PhysRevB.64.165411> (visited on 10/10/2016).
- Naoki Komatsu, Li Zhao (2011). "Chromatographic Separation of Highly Soluble Diamond Nanoparticles Prepared by Polyglycerol Grafting". In: Neu, E. et al. (2013). "Low temperature investigations and surface treatments of colloidal narrowband fluorescent nanodiamonds". en. In: *Journal of Applied Physics* 113.20, p. 203507. ISSN: 00218979. DOI: 10.1063/1.4807398. URL: <http://scitation.aip.org/content/aip/journal/jap/113/20/10.1063/1.4807398> (visited on 10/10/2016).
- Orbach, R. (1961). "Spin-Lattice Relaxation in Rare-Earth Salts". en. In: *Proceedings of the Royal Society A: Mathematical, Physical and Engineering Sciences* 264.1319, pp. 458–484. ISSN: 1364-5021, 1471-2946. DOI: 10.1098/

- rspa.1961.0211*. URL: <http://rspa.royalsocietypublishing.org/cgi/doi/10.1098/rspa.1961.0211> (visited on 10/10/2016).
- Osswald, Sebastian et al. (2006). "Control of sp<sub>2</sub>/sp<sub>3</sub> Carbon Ratio and Surface Chemistry of Nanodiamond Powders by Selective Oxidation in Air". In: *Journal of the American Chemical Society* 128.35, pp. 11635–11642. ISSN: 0002-7863. DOI: [10.1021/ja063303n](https://doi.org/10.1021/ja063303n). URL: <http://dx.doi.org/10.1021/ja063303n> (visited on 10/10/2016).
- Ristein, J. (2000). "Electronic properties of diamond surfaces — blessing or curse for devices?" In: *Diamond and Related Materials* 9.3–6, pp. 1129–1137. ISSN: 0925-9635. DOI: [10.1016/S0925-9635\(99\)00316-7](https://doi.org/10.1016/S0925-9635(99)00316-7). URL: <http://www.sciencedirect.com/science/article/pii/S0925963599003167> (visited on 10/10/2016).
- Rogers, Lachlan J. et al. (2013). "Multiple intrinsically identical single photon emitters in the solid state". In: *arXiv:1310.3804 [cond-mat, physics:physics, physics:quant-ph]*. URL: <http://arxiv.org/abs/1310.3804> (visited on 06/06/2014).
- Rogers, Lachlan J. et al. (2014a). "All-optical initialization, readout, and coherent preparation of single silicon-vacancy spins in diamond". In: *Physical Review Letters* 113.19. arXiv: 1410.1355. ISSN: 0031-9007, 1079-7114. DOI: [10.1103/PhysRevLett.113.197601](https://doi.org/10.1103/PhysRevLett.113.197601). URL: <http://arxiv.org/abs/1410.1355> (visited on 11/25/2014).
- Rogers, Lachlan J. et al. (2014b). "Electronic structure of the negatively charged silicon-vacancy center in diamond". In: *Physical Review B* 89.23, p. 235101. DOI: [10.1103/PhysRevB.89.235101](https://doi.org/10.1103/PhysRevB.89.235101). URL: <http://link.aps.org/doi/10.1103/PhysRevB.89.235101> (visited on 06/03/2014).
- Santori, Charles et al. (2006). "Coherent population trapping in diamond N-V centers at zero magnetic field". en. In: *Optics Express* 14.17, p. 7986. ISSN: 1094-4087. DOI: [10.1364/OE.14.007986](https://doi.org/10.1364/OE.14.007986). URL: <https://www.osapublishing.org/oe/abstract.cfm?uri=oe-14-17-7986> (visited on 10/10/2016).
- Scott, P. L. (1962). "Spin-Lattice Relaxation in Some Rare-Earth Salts at Helium Temperatures; Observation of the Phonon Bottleneck". In: *Physical Review* 127.1, pp. 32–51. DOI: [10.1103/PhysRev.127.32](https://doi.org/10.1103/PhysRev.127.32).
- Stacey, A. et al. (2012). "Depletion of nitrogen-vacancy color centers in diamond via hydrogen passivation". In: *Applied Physics Letters* 100.7, p. 071902. ISSN: 0003-6951, 1077-3118. DOI: [10.1063/1.3684612](https://doi.org/10.1063/1.3684612). URL: <http://scitation.aip.org/content/aip/journal/apl/100/7/10.1063/1.3684612> (visited on 12/04/2014).
- T. Gaebel, C.Bradac (2012). "Size-reduction of nanodiamonds via air oxidation". In: *Diamond and Related Materials* 21, pp. 28–32. DOI: [10.1016/j.diamond.2011.09.002](https://doi.org/10.1016/j.diamond.2011.09.002). URL: <http://www.sciencedirect.com/science/article/pii/S0925963511003116>.
- Wang, Chunlang et al. (2006). "Single photon emission from SiV centres in diamond produced by ion implantation". en. In: *Journal of Physics B: Atomic, Molecular and Optical Physics* 39.1, p. 37. ISSN: 0953-4075. DOI: [10.1088/0953-4075/39/1/005](https://doi.org/10.1088/0953-4075/39/1/005). URL: <http://stacks.iop.org/0953-4075/39/i=1/a=005> (visited on 10/11/2016).
- Wolcott, Abraham et al. (2014). "Surface Structure of Aerobically Oxidized Diamond Nanocrystals". In: *The Journal of Physical Chemistry C* 118.46, pp. 26695–26702. ISSN: 1932-7447. DOI: [10.1021/jp506992c](https://doi.org/10.1021/jp506992c). URL: <http://dx.doi.org/10.1021/jp506992c> (visited on 12/03/2014).

Yeap, Weng Siang, Shiming Chen, and Kian Ping Loh (2009). "Detonation Nanodiamond: An Organic Platform for the Suzuki Coupling of Organic Molecules". In: *Langmuir* 25.1, pp. 185–191. ISSN: 0743-7463. DOI: [10.1021/la8029787](https://doi.org/10.1021/la8029787). URL: <http://pubs.acs.org/doi/abs/10.1021/la8029787> (visited on 10/10/2016).